RESEARCH LABORATORY

Terminal Ballistic Evaluation of a Candidate 0.60-Caliber Electromagnetically Launched Long-Rod Penetrator

Timothy G. Farrand

ARL-MR-104 September 1993

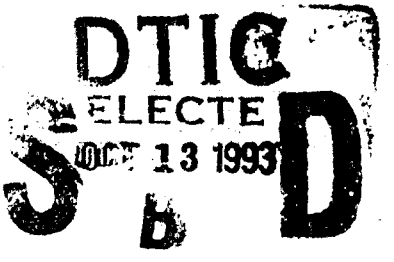

NOTICES

Destroy this report when it is no longer needed. DO NOT return it to the originator.

Additional copies of this report may be obtained from the National Technical Information Service, U.S. Department of Commerce, 5285 Port Royal Road, Springfield, VA 22161.

The findings of this report are not to be construed as an official Department of the Army position, unless so designated by other authorized documents.

The use of trade names or manufacturers' names in this report does not constitute indorsement of any commercial product.

REPORT DOCUMENTATION PAGE

Form Approved
OMB No 0704-0188

1. AGENCY USE ONLY (Leave blank)	2. REPORT DATE	3. REPORT TYPE AND DATES COVERED
	September 1993	Final, Aug 90–Aug 92

4. TITLE AND SUBTITLE

Terminal Ballistic Evaluation of a Candidate 0.60-Caliber Electromagnetically Launched Long-Rod Penetrator

5. FUNDING NUMBERS

FOA 2999AAHD1
WO# 44031-057-62

6. AUTHOR(S)

Timothy G. Farrand

7. PERFORMING ORGANIZATION NAME(S) AND ADDRESS(ES)

U.S. Army Research Laboratory
ATTN: AMSRL-WT-TD
Aberdeen Proving Ground, MD 21005-5066

8. PERFORMING ORGANIZATION REPORT NUMBER

9. SPONSORING / MONITORING AGENCY NAME(S) AND ADDRESS(ES)

U.S. Army Research Laboratory
ATTN: AMSRL-OP-CI-B (Tech Lib)
Aberdeen Proving Ground, MD 21005-5066

10. SPONSORING / MONITORING AGENCY REPORT NUMBER

ARL-MR-104

11. SUPPLEMENTARY NOTES

12a. DISTRIBUTION / AVAILABILITY STATEMENT

Approved for public release; distribution is unlimited.

12b. DISTRIBUTION CODE

13. ABSTRACT *(Maximum 200 words)*

A candidate 0.60-cal. armor-piercing, fin-stabilized, discarding armature, kinetic energy penetrator, to be fired from an electromagnetic (EM) launcher, was evaluated for its terminal ballistic performance against rolled homogeneous armor (RHA). A limited data set was also generated for high hardness armor. The candidate design is similar to one generated from an empirically based optimization study. The study considered launch, flight, and terminal ballistic performance from a 0.60-cal. electromagnetic gun. Projected performance of the projectile at range was generated using the system parameters (muzzle velocity and aerodynamic retardation) combined with the perforation ability against RHA.

14. SUBJECT TERMS

electromagnetic launcher, long-rod penetrator penetration, perforation, rolled homogeneous armor, high hardness armor, kinetic energy penetrator, 0.60 caliber, kinetic energy

15. NUMBER OF PAGES

65

16. PRICE CODE

17. SECURITY CLASSIFICATION OF REPORT	18. SECURITY CLASSIFICATION OF THIS PAGE	19. SECURITY CLASSIFICATION OF ABSTRACT	20. LIMITATION OF ABSTRACT
UNCLASSIFIED	UNCLASSIFIED	UNCLASSIFIED	SAR

INTENTIONALLY LEFT BLANK.

ACKNOWLEDGMENTS

The author wishes to acknowledge Mrs. Wendy Leonard and Dr. Lee Magness for their continued assistance in data reduction and analysis. He also wishes to thank the ARL Range 110 technicians who performed the actual testing including, Mrs. Eleanor Deal, Mr. Bernard McKay, Mr. Jack Koontz, Mr. Maurice Clarke, Mr. Vaughn Torbert, and Mr. Richard English. Finally, Mr. Alexander Zielinski, in addition to supplying the needed aeroballistic data, was instrumental in arranging the funding for this terminal ballistic evaluation. Funding was provided from the Armament Research Development and Engineering Center (ARDEC), Close Combat Armaments Center (CCAC), with the continued support of Messrs. H. Kahn and H. Moore.

INTENTIONALLY LEFT BLANK.

TABLE OF CONTENTS

		Page
	ACKNOWLEDGMENTS	iii
	LIST OF FIGURES	vii
	LIST OF TABLES	ix
1.	INTRODUCTION	1
2.	PROJECTILE DESCRIPTION	1
3.	TARGET MATRIX	3
4.	TEST PROCEDURE	5
5.	TERMINAL BALLISTIC RESULTS	7
5.1	RHA Semi-Infinite Target	7
5.2	Finite Target	7
6.	DISCUSSION	8
6.1	Semi-Infinite Target	8
6.2	Finite Target	11
7.	SYSTEM PERFORMANCE	14
8.	CONCLUSIONS	18
9.	REFERENCES	19
	APPENDIX A: AN EXPLANATION OF FIGURES AND TABLES OF INDIVIDUAL FIRING DATA	21
	APPENDIX B: TABULATIONS OF INDIVIDUAL SHOT DATA	35
	DISTRIBUTION LIST	63

INTENTIONALLY LEFT BLANK.

LIST OF FIGURES

Figure		Page
1.	Photographs of the 0.60-cal. APFSDA projectile package	2
2.	Schematic comparison of EM-launched tungsten penetrator and TBS	4
3.	Terminal ballistic launch package with surrogate projectile	o
4.	Plot of semi-infinite penetration as a function of velocity (total impact yaw noted)	9
5.	Prints of radiographs from semi-infinite blocks	10
6.	Line of Sight (LOS) RHA penetration and perforation thickness for the 0.60-cal. TBS	12
7.	Comparison of various nose shapes into semi-infinite RHA at 70.5° obliquity	13
8.	Comparison of perforation of HHA and RHA targets	15
A-1.	Illustration of primary preimpact and postimpact radiographic measures	30
A-2.	Illustration of target plate measures - partial penetration	31
A-3.	Illustration of target plate measures - complete penetration	31
A-4.	Illustration of radiographic behind-armor debris measures	32
A-5.	Illustration of between-plate measures in spaced array target	33
A-6.	Illustration of penetration measures in semi-infinite target	34
B-1.	V_S-V_R curve for the 0.60-cal. TBS against 50.8-mm RHA at 0° obliquity	42
B-2.	V_S-V_R curve for the 0.60-cal. TBS against 19.05-mm RHA at 57° obliquity	46
B-3.	V_S-V_R curve for the 0.60-cal. TBS against 31.75-mm RHA at 57° obliquity	50
B-4.	V_S-V_R curve for the 0.60-cal. TBS against 12.7-mm RHA at 70.5° obliquity	54
B-5.	V_S-V_R curve for the 0.60-cal. TBS against 12.7-mm HHA at 70.5° obliquity	61

INTENTIONALLY LEFT BLANK.

LIST OF TABLES

Table		Page
1.	Semi-Infinite RHA Terminal Ballistic Results	7
2.	Limit Velocities for the Finite Thickness Targets	8
3.	Estimated Normal Perforation Thickness (mm) for the 0.60-cal. APFSDA Against RHA	17
B-1.	Individual Shot Data Tabulation for the 0.60-cal. TBS Against Semi-Infinite RHA at 0° Obliquity	37
B-2.	Individual Shot Data Tabulation for the 0.60-cal. TBS Against 50.8-mm RHA at 0° Obliquity	39
B-3.	Individual Shot Data Tabulation for the 0.60-cal. TBS Against 19.05-mm RHA at 57° Obliquity	43
B-4.	Individual Shot Data Tabulation for the 0.60-cal. TBS Against 31.75-mm RHA at 57° Obliquity	47
B-5.	Individual Shot Data Tabulation for the 0.60-cal. TBS Against 12.7-mm RHA at 70.5° Obliquity	51
B-6.	Individual Shot Data Tabulation for the 0.60-cal. TBS Against 19.05-mm HHA at 57° Obliquity	55
B-7.	Individual Shot Data Tabulation for the 0.60-cal. TBS Against 12.7-mm HHA at 70.5° Obliquity	58

INTENTIONALLY LEFT BLANK.

1. INTRODUCTION

A parametric paper study using empirical equations for launch, aerodynamic flight, and terminal ballistic characteristics for the development of the 0.60-cal. armor-piercing, fin-stabilized, discarding armature (APFSDA) launched from an electromagnetic (EM) gun system was performed by Mr. Alexander Zielinski (Engineering Physics Branch of the Terminal Ballistic Division of the U.S. Army Ballistic Research Laboratory).* Design parameters fixed in the study include a 0.60-cal. barrel length of 1.6 m, an armature length of 1.6-cal., and an engagement range of 1,500 m for a 0° obliquity rolled homogeneous armor (RHA) target (Zielinski 1991).

A candidate projectile package from the study was developed. The study utilized a methodology by which required projectile dimensions are determined from launch velocity, muzzle energy, and structural and thermal loads. The 0.60-cal. gun system has projectile performance specified as a 32-g mass launched at 2,000 m/s (Kitzmiller et al. 1991). Iterations for the terminal ballistic surrogate (TBS) design launch mass and their velocity trade-offs above and below the 0.60-cal. specifications were used to determine the substantial performance obtained by a projectile package launched at 1,800 m/s and 55 kJ of total muzzle kinetic energy. The following is the analysis of this type of projectile against RHA and some evaluations of high hardness armor (HHA).

A surrogate projectile was designed for the terminal ballistic evaluation to lower the manufacturing costs and to ease the launchability from the terminal ballistic laboratory gun system. The TBS was designed to reflect the performance of the actual projectile without incorporating many of the intricate design features that do not influence the penetration.

2. PROJECTILE DESCRIPTION

Figure 1 is a photograph of the 0.60-cal. APFSDA launch package. It has supercaliber grooves for transferring the load developed in the aluminum sabot/armature to the sub-projectile. A polypropylux obturator encompasses the front of the aluminum armature which, after exiting the barrel (free flight), is discarded. At the rear section there is a long reduced threaded region for attaching the fin assembly. The

---

* On 30 September 1992, the U.S. Army Ballistic Research Laboratory (BRL) was deactivated and subsequently became part of the U.S. Army Research Laboratory (ARL) on 1 October 1992.

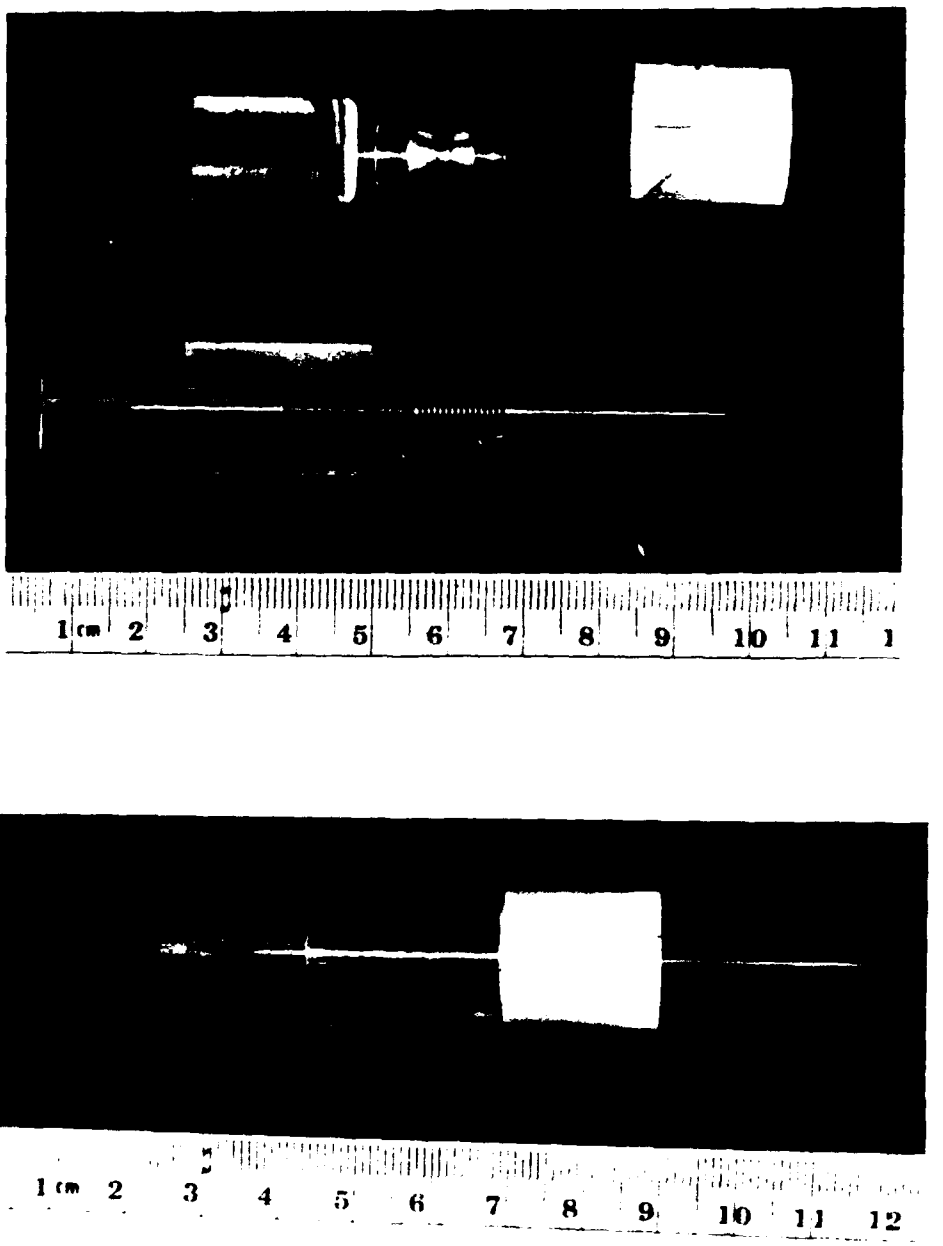

Figure 1. Photographs of the 0.60-cal. APFSDA projectile package.

front of the penetrator is a sharp conical nose (10° half-angle) designed as a compromise between low aeroballistic drag and deleterious terminal ballistic effects at obliquity. As can be seen, this is a very intricate design which would require extensive machining. For terminal ballistic evaluations, the detail in supercaliber grooves and reduced fin assembly region is not required. The nose shape, however, is needed to accurately define the terminal ballistic performance, especially for oblique targets.

By eliminating the details required for the EM launch and free-flight, a smooth right circular cylinder penetrator of equal length and diameter with a conical nose was substituted to use in the terminal ballistic evaluation. Figure 2, a schematic comparing both subprojectiles, shows that the overall length, diameter, and mass are very similar. The increase in mass from filling in the reduced section for the fin assembly is compensated for by the decrease in mass from eliminating the supercaliber grooves. The TBS design becomes much easier to launch in the laboratory terminal ballistic range and less expensive to produce.

The projectile is manufactured from a tungsten heavy alloy (93%W-4.9%Ni-2.1%Fe) which was moderately cold worked. The nominal mechanical properties of the penetrator material (as given from the manufacturer, Teledyne Firth Sterling) are as follows: density - 17.6 g/cm^3, ultimate tensile strength - 185 ksi, tensile yield strength - 150 ksi, minimum elongation - 8%, and hardness - Rc45.

3. TARGET MATRIX

The baseline terminal ballistic performance is characterized with RHA, Mil-Spec-12560G. RHA plates vary in hardness with thickness. Due to the rolling nature of the manufacturing process (thinner plates are rolled for a longer period of time), the hardness increases as the thickness decreases.

Initial terminal ballistic testing begins by determining the depth of penetration into semi-infinite armor, an armor of sufficient thickness and width so the depth of penetration is not influenced by any free surface effects. For these tests, target thicknesses of 4–6 in (101.6–152.4 mm) were used, BHN 286-302. The depth is measured by taking a high-powered radiograph of the block and/or sectioning the block along the shot line. Once the semi-infinite performance is quantified, the performance against finite thickness plates at normal impacts is evaluated. This helps to ascertain the rear free surface effects and separate the penetration and perforation effects. Finally, the effect of obliquity is examined by varying the

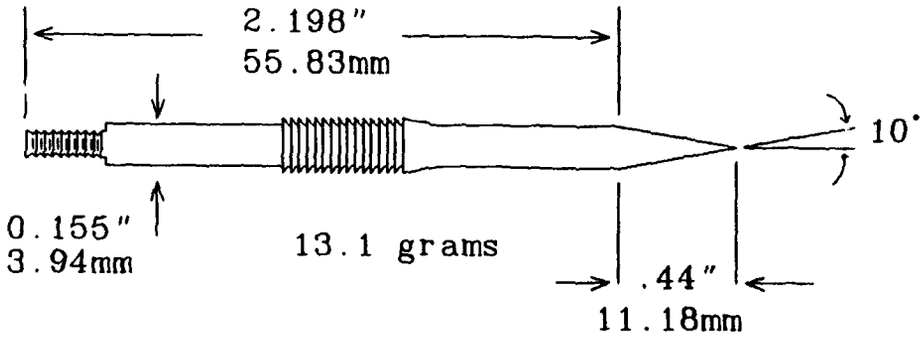

a. EM-launched tungsten penetrator.

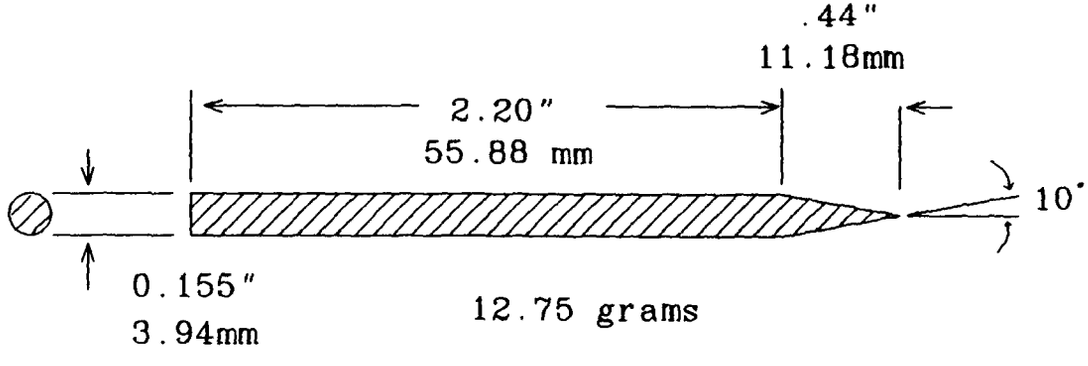

b. TBS.

Figure 2. Schematic comparison of EM-launched tungsten penetrator and TBS.

thickness and obliquity of the finite RHA plates. The thinner plates used for the finite test have BHN values ranging from 302 to 364.

A similar analysis is used for HHA, Mil-Spec-46100C. HHA plates are heat treated to achieve their desired hardness (BHN 512) and are, therefore, the same hardness for all thickness plates. Because of the heat treatment process, it is difficult to form HHA plates of thicknesses greater than 1.5 in (38.1 mm) and with a consistent through thickness hardness. The targets evaluated in this test were less than 1.5 in thick, (1/2 in [12.7 mm] and 3/4 in [19.01 mm]). The size of the target matrix for the HHA was limited to two finite thickness targets due to the funding and availability of supplies.

4. TEST PROCEDURE

The actual EM launch system was not required to evaluate the terminal ballistic performance of the penetrator. Rather, the standard launch system for terminal ballistic evaluation in the laboratory test range, ARL Range 110, was used.

A 10-ft-long (3.05-m) smoothbore barrel, which gives smooth accelerations for a large range of velocities, was implemented. A four-piece polypropylux sabot and a steel pusher disc, recessed in a polypropylux obturator, make up the launch package (shown, along with the TBS rod, in Figure 3). After exiting the gun tube, the sabot separates from the rod very quickly, and the pusher and obturator follow the penetrator to the target. Since a deflector was not used, the pusher disc and obturator impact the target after the penetrator-target interaction is complete.

Preimpact measures are generated from a flash-radiograph system. While in free-flight, the penetrator breaks an electrical screen starting a timer that pulses two preimpact orthogonal flash radiographs. These radiographs capture images of the penetrator, just prior to impacting the target. From the time delay between the flashes and fiducial lines on the film, the velocity and orientation of the impacting penetrator can be determined (Grabarek and Herr 1976). In addition, for the finite thickness plates, a similar break screen arrangement is located on the back face of the target to capture two images (solely in the vertical plane) of the exiting behind-armor target debris and residual penetrator. These images are used to estimate residual penetrator velocity, mass, and departure angle. They can also be used to evaluate the behind-armor lethality of the debris. Various preshot and in-flight parameters measured are detailed in Appendix A.

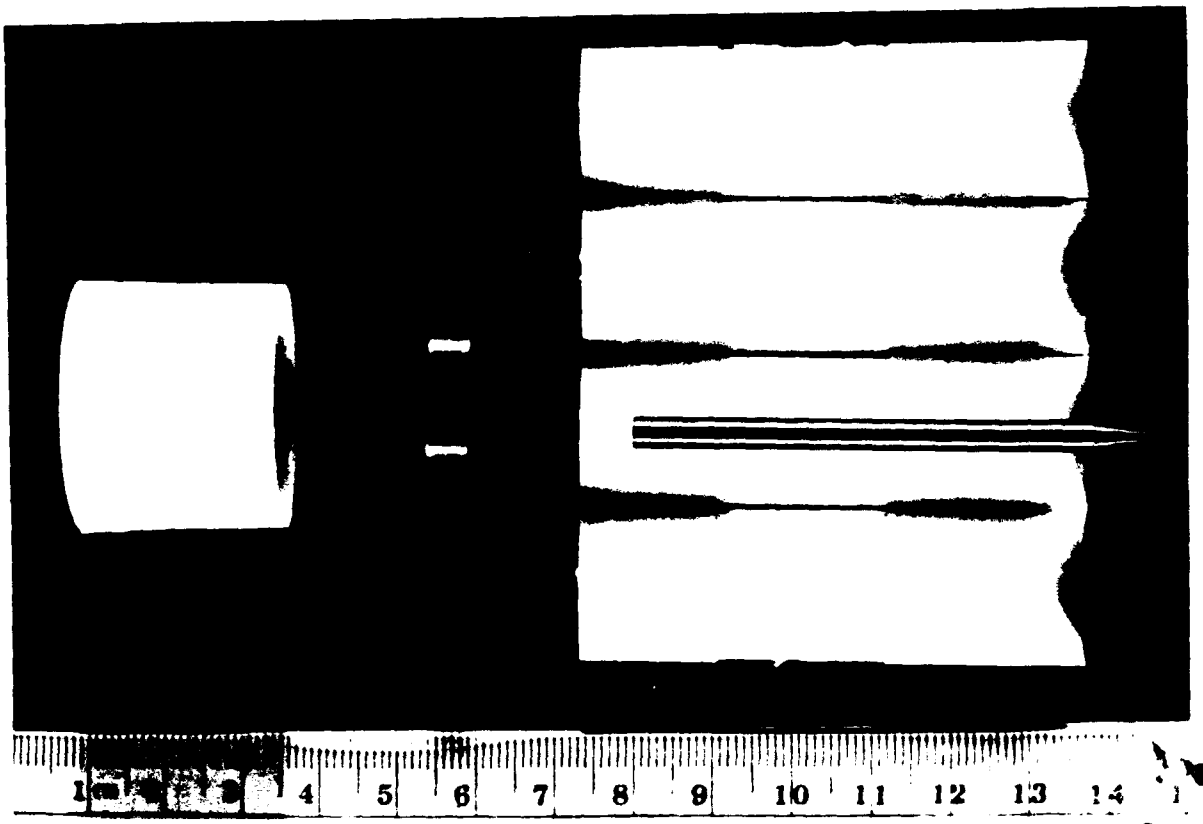

Figure 3. Terminal ballistic launch package with surrogate projectile.

For the finite targets, the impact velocity and residual velocity data pairs are used in an empirically fitted equation (1) to calculate the limit velocity for the target (Lambert and Jonas 1976). The limit velocity is the maximum impact velocity where the residual velocity is zero. The empirical parameters A, P, and the V_L are determined through a nonlinear least square fit to Equation 1. Sample V_S–V_R data plots to Equation 1 are shown in Appendix B.

$$V_R = A(V_S^P - V_L^P)^{1/P}, \quad (1)$$

where

V_R = residual velocity (m/s),

V_S = striking velocity (m/s),

V_L = limit velocity (m/s) to be determined,

A and P = empirical fitting parameters.

Postmortem measures of all target blocks are also recorded (described in detail in Appendix A). Depending on whether the shot was a complete perforation or a partial penetration, the entrance, exit,

depth of penetration, and/or center hole dimensions for the finite targets are measured. To evaluate the penetration channel parameters (depth, volume, diameter) of the semi-infinite target blocks, a high-powered radiograph is taken through the target. The typical method of cross-sectioning the semi-infinite block is used after the radiographic method because, for the small diameter rod, the penetration channel is so narrow it is difficult to cut at the exact half-section. By using both methods, cross sectioning and radiographs, an accurate assessment of the penetration channel is possible.

5. TERMINAL BALLISTIC RESULTS

5.1 RHA Semi-Infinite Target. A summary of the semi-infinite results is presented in Table 1. The final depth of penetration (mm) for the seven shots and their preimpact measures, yaw, striking velocity, and mass, are shown. A detailed listing of the individual shot data appears in Appendix B.

Table 1. Semi-Infinite RHA Terminal Ballistic Results

Shot No.	Total Yaw (°)	Striking Velocity (m/s)	Mass (g)	Penetration (mm)
1137	1.46	1,122	12.81	26.2
1136	1.27	1,220	12.82	30.0
1138	0.75	1,260	12.83	33.8
1142	2.02	1,485	12.77	49.0
1139	2.30	1,490	12.81	45.2
1140	0.90	1,699	12.81	65.5
1141	0.79	1,861	12.76	75.7

5.2 Finite Target. Table 2 is a listing of the limit velocities determined for the finite targets evaluated. The RHA targets consisted of a 0° obliquity plate, 57° obliquity plates of two thicknesses, and a 70.5° obliquity plate. Limited testing supplies allowed for evaluation of only two HHA targets at obliquities of 57° and 70.5°. The thickness and obliquity for these targets match some of those for the RHA, to possibly compare the performance of HHA to that of RHA. Again, a detailed individual shot tabulation for each test series appears in Appendix B.

The RHA data were fairly clean (good impacts and respectable fits to Equation 1), consisting of seven to eight shots each. In contrast, the HHA data are not as clean. One series needed 12 shots (there were many bad yawed impacts, and the data were still very scattered). The final data (19.05-m HHA at 57° obliquity) series was terminated as the supplies were exhausted. An estimate was made for the ballistic limit velocity by averaging the only partial penetration and the lowest complete perforation (a two shot V_{50} with a spread of 2 m/s). The large scatter in the residual velocities (which is more typical for HHA plates) prevented the fitting routine from calculating the limit velocity.

Table 2. Limit Velocities for the Finite Thickness Targets

Material	Normal Thickness (mm)	Obliquity (°)	Average Hardness (BHN)	Line of Sight Thickness (mm)	Limit Velocity (m/s)
RHA	50.8	0	321	50.8	1,483
RHA	19.05	57	360	35.0	1,220
RHA	31.75	57	330	58.3	1,716
RHA	12.7	70.5	364	38.1	1,262
HHA	19.05	57	512	35.0	1,330
HHA	12.7	70.5	512	38.1	1,430

6. DISCUSSION

6.1 Semi-Infinite Target. A plot of the semi-infinite data, including the corresponding total yaw, is shown in Figure 4. As can be seen, the impact with the highest yaw (2.3°) falls below the good impact data. The point with 2.0° yaw, however, is very near the norm. This implies, for a 0° obliquity target, yaw up to approximately 2.0° will not greatly affect the final depth of penetration. Equation 2 is a geometric calculation of the critical yaw (Silsby et al. 1983), yaw large enough for the tail end of the rod to have physical impact on the edge of the penetration channel, and is given as,

$$\gamma_C = \sin^{-1}\left[\frac{(H - D)/2}{L}\right], \qquad (2)$$

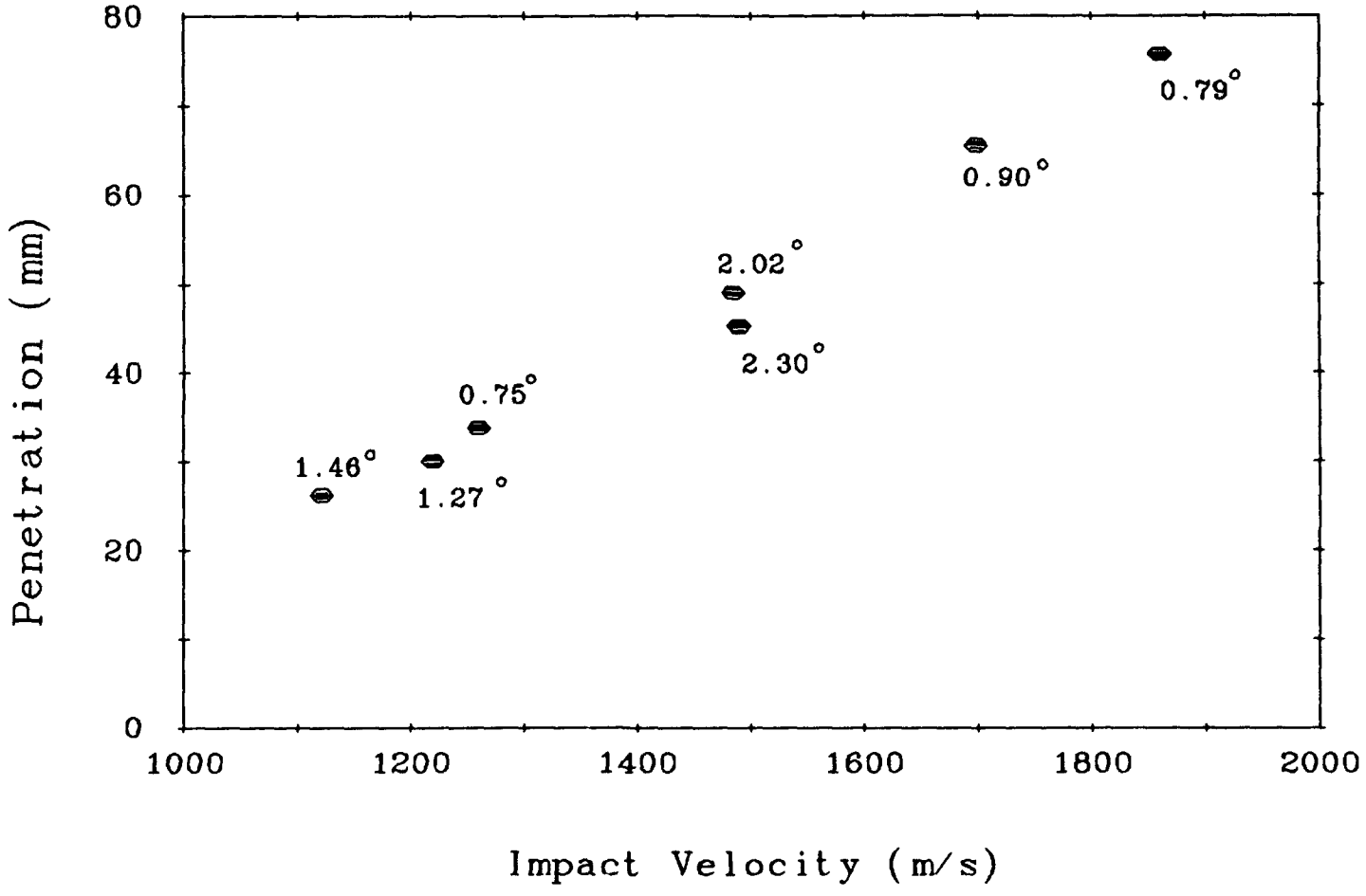

Figure 4. Plot of semi-infinite penetration as a function of velocity (total impact yaw noted).

where

γ_C = geometric critical yaw (deg),

H = diameter of penetration channel (mm),

D = original diameter of penetrator (mm),

L = original length of penetrator (mm).

Using the dimensions of the rod diameter of 3.9 mm and length of 56 mm (not including the conical nose), and the average entrance hole diameter (6 mm), a critical yaw is calculated to be 1.07°. This is lower than the 2.0° yaw value estimated from the plot.

The critical yaw equation (2) (Silsby et al. 1983) was developed with hemi-nose penetrators where the entrance hole is approximately the same diameter as the constant diameter portion.

The geometric calculation determines the value where the tail first interferes with the edge of the channel. The plot implies that minor interference does not affect the final depth of penetration substantially. Also, the conical nose shape of the rod produces a narrow entrance hole which widens as the depth increases. Copies of two radiographic images for the semi-infinite targets are shown in Figure 5. As described, the entrance hole is narrow as the target material is displaced just enough to allow the remaining rod to pass through. As the constant diameter of the rod is being eroded, the channel diameter widens (Farrand and Zook 1992). If the critical yaw was recalculated using this constant diameter channel portion (7.5 mm) instead of the narrow entrance hole region, the critical yaw becomes 1.8°. This tends to agree more with the plotted data.

Shot No. 1137 Shot No. 1139

Figure 5. Prints of radiographs from semi-infinite blocks.

6.2 Finite Target. A plot of line-of-sight (LOS) thickness as a function of velocity for both the semi-infinite and finite thickness RHA data is shown in Figure 6. An estimated curve for the semi-infinite data is constructed, with the highest yaw data lying somewhat below the curve.

The distance between the 0° finite target and the 0° semi-infinite target curves depicts the added thickness the projectile can perforate over its depth of penetration at the same velocity. This additional perforation thickness is due to failure of the rear free surface, also known as the plugging phase. The size of the plug is dependent on the penetrator diameter and target material. For RHA and the small diameter rod, this appears to be approximately one half the original rod diameter or 2 mm.

A typical long rod penetrator can perforate more LOS thickness RHA as the obliquity of the finite target is increased. As the penetrator creates a channel through the finite target, it tends to take the path of least resistance. For high-obliquity targets, this tends to be towards the normal of the target, decreasing the effective LOS thickness of the target. If the penetrator has a conical nose shape, the penetrator will deflect on the target front surface and delay the perforation process. In addition, once the penetration begins for the higher obliquity targets, its channel is more parallel to the plate, so its effective thickness is increased. This deflection of the penetration channel is depicted in Figure 7 (Farrand and Zook 1992). Figure 7 shows the cross section of semi-infinite plates at 70.5° obliquity after being impacted by various nose shape, L/D = 10 rods, at the same nominal velocity.

The conical nose shape of the EM long rod did experience deflection for the higher obliquity targets. If the target is relatively thin, however, this deflection is compensated for by the plugging or break out of the rear free surface. So at the lower velocity (1,250 m/s), the EM subprojectile LOS thickness does not change considerably with a change in obliquity. As the thickness of the target is increased, the deflection is more of a factor because the penetration phase contributes much more than the plugging phase. As can be seen from Figure 6, at the higher velocity and/or thicker target, the penetrator can actually penetrate further into semi-infinite armor than it can perforate at 57° obliquity.

Although penetration into semi-infinite HHA data were not accumulated in these tests, past experiments with similar caliber projectiles have shown that HHA is harder to penetrate than RHA (Magness et al. 1988). Also, the plugging phase is much larger in HHA. Because the plug is a function of the penetrator diameter, its contribution for the 0.60-cal. long rod penetrator is probably minor.

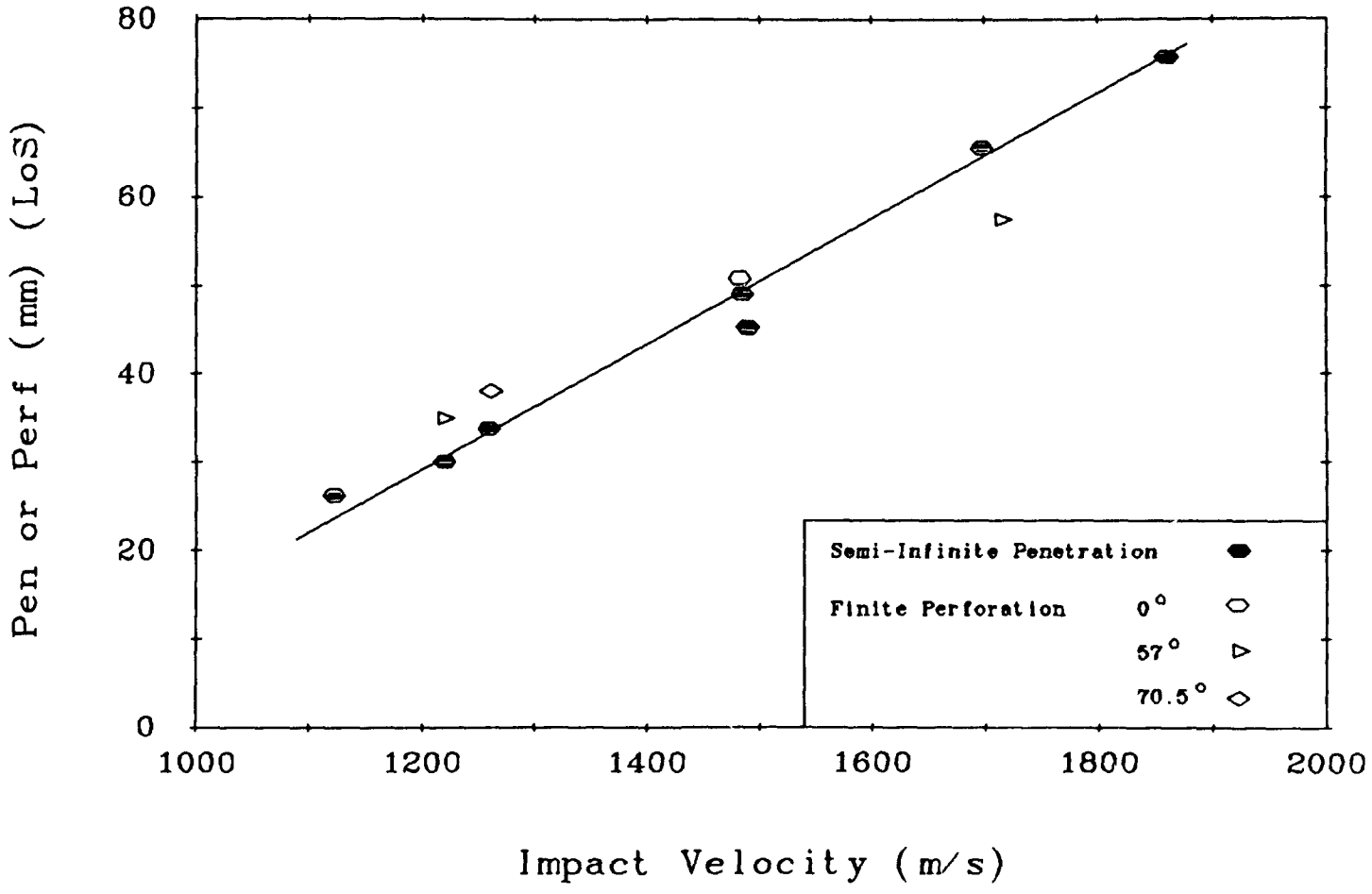

Figure 6. Line of sight (LOS) RHA penetration and perforation thickness for the 0.60-cal. TBS.

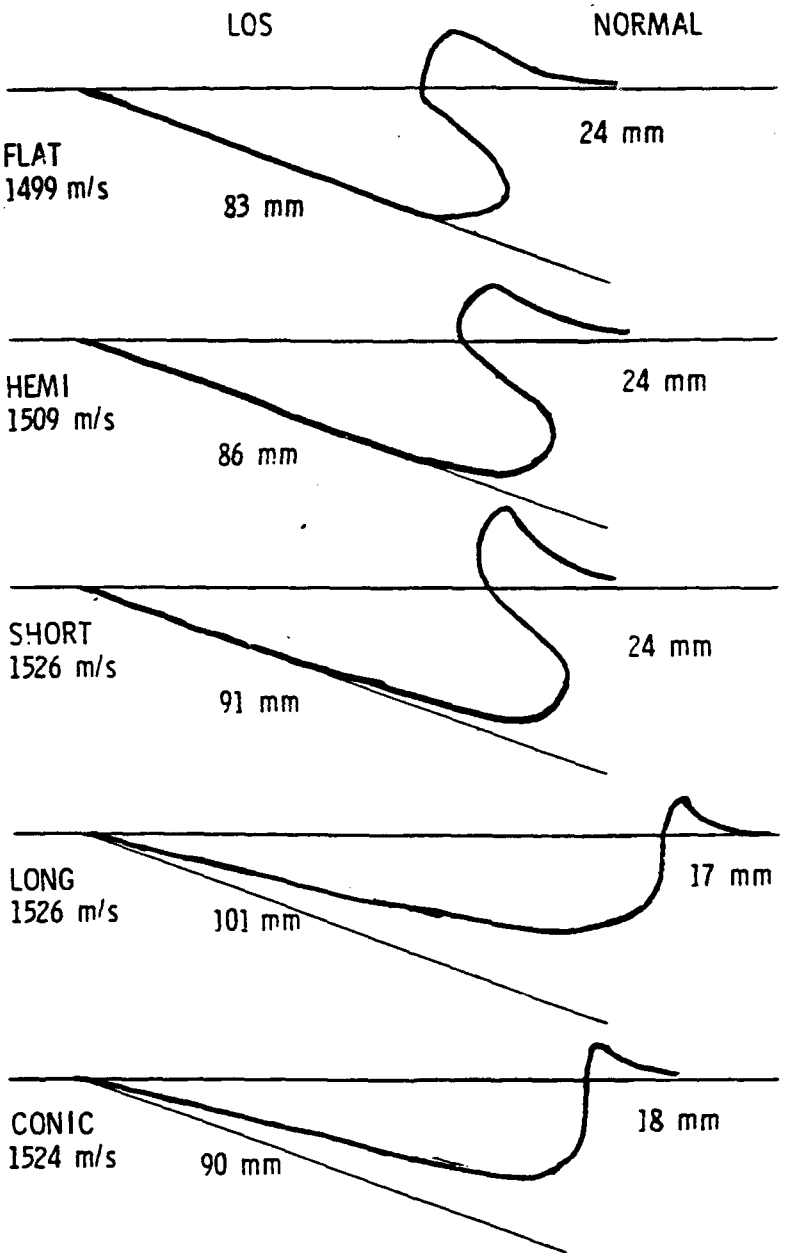

Figure 7. Comparison of various nose shapes into semi-infinite RHA at 70.5° obliquity.

Figure 8 is a plot of the LOS thickness for the two HHA targets and also the same thickness and obliquity RHA targets. The decrease in penetration ability and, probably, increased deflection (due to the higher hardness) are reflected in the much higher limit velocities for the equivalent thickness and obliquity HHA targets. In addition, the much larger gap between the limit velocities for the 57° and 70.5° HHA targets as compared to that of the RHA targets, implies that the HHA plate deflects the rod even more at the higher obliquities.

7. SYSTEM PERFORMANCE

From the terminal ballistic data generated, an overall model to estimate the perforation ability of the penetrator over a range of velocities and obliquities can be constructed. A common model used in describing the perforation by small-caliber ammunition is the Grabarek model, shown in Equation 3. It is an empirical model derived from the De Marre formulation (Grabarek 1971).

$$T_N \cos^{\beta}(\theta) = D \left(\frac{M V^2}{A D^3} \right)^{1/\alpha}, \tag{3}$$

where

T_N = normal target thickness (mm),
M = mass of penetrator (g),
D = diameter of penetrator (mm),
Θ = target obliquity (deg),
V = impact velocity (m/s),
A, α, β = empirical fitting parameters.

As can be seen, the model is dependent on mass, diameter, and impact velocity. There are three fitting parameters: A, alpha (α), and beta (β). Beta reflects the effect of obliquity. If beta equals 1, then the LOS thickness that can be perforated is constant, regardless of obliquity. If beta is less than 1, then the penetrator can perforate a greater LOS thickness at obliquity than at zero. Conversely, if beta is greater than 1, it will perforate less LOS thickness at obliquity. Where dependence on obliquity is not as simplistic and straightforward, additional modifications to beta are applied. By making beta a function of obliquity and velocity, it allows the obliquity effect to vary with thickness.

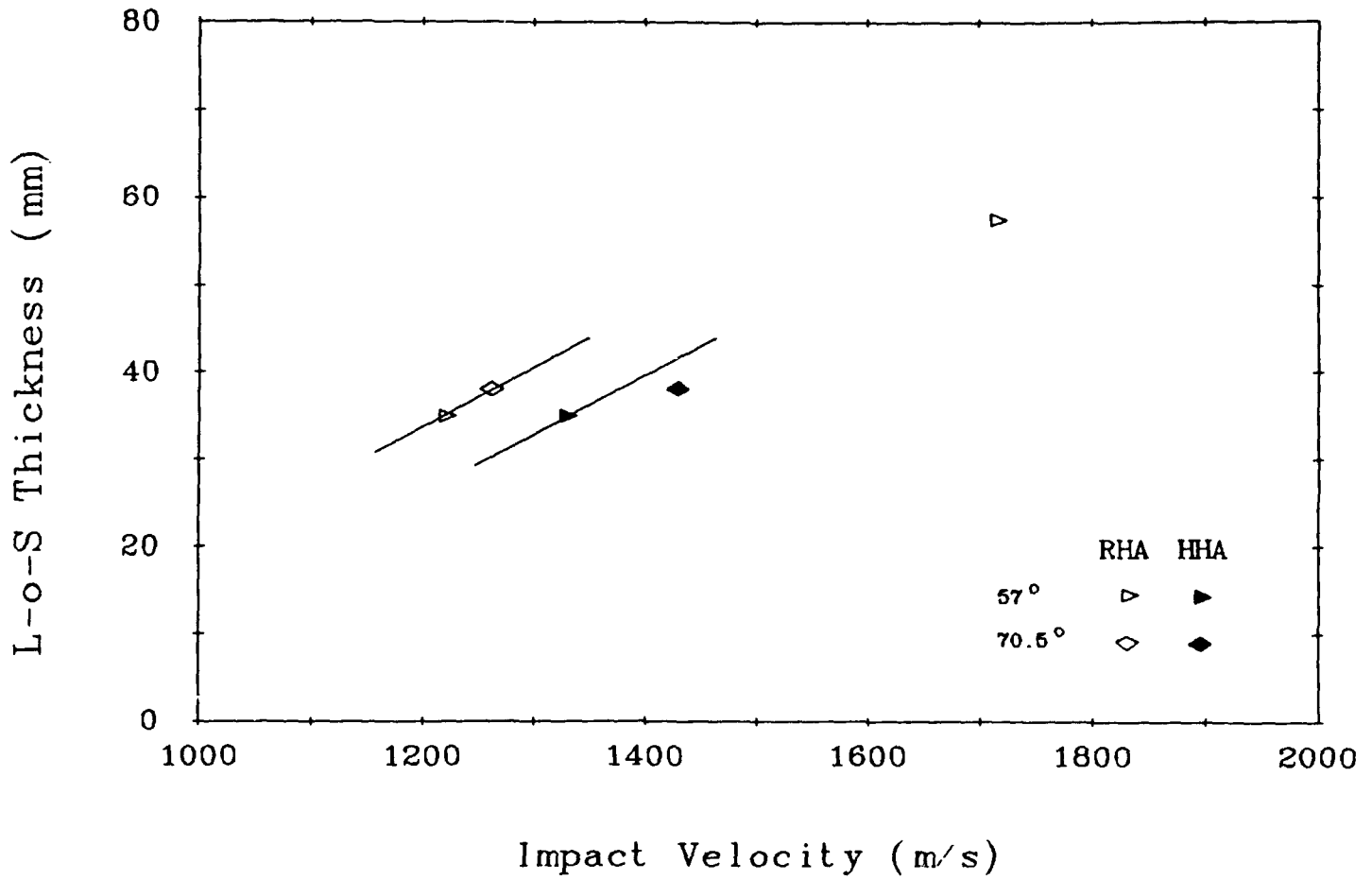

Figure 8. Comparison of perforation of HHA and RHA targets.

For the complicated obliquity effects observed with the 0.60-cal. TBS, a complex fit to the beta value was developed. From this formulation, the drop-off in performance with increase in obliquity and ever greater decrease in performance with thicker targets (higher velocity) is modeled. Since this is a force fit to the data, it is recommended that it not be extrapolated far beyond the bounds of the actual data. A mass of 12.8 g and a diameter of 3.94 mm were used in the routine to derive the best fit for the empirical values; A = 38,050, α = 0.981, and the beta function described in Equation 4. Beta from this equation ranges from 0.934 for obliquities less than 57° and velocities less than 1,200 m/s, to greater than 1.0 at higher velocities and obliquities (i.e., at a velocity of 1,600 m/s and obliquity of 70.5°, beta is 1.20).

$$\beta = 0.934 \qquad \text{for } \theta < 57° \text{ and } V < 1200$$

$$\beta(\theta,V) = 0.934 + (0.001185)(\theta - 57) + (0.0006129)(V - 1200) \qquad (4)$$

By incorporating the predicted launch and flight characteristics (Zielinski 1991) and the terminal ballistic fit just described, the range at which a target (thickness and obliquity) can be defeated is easily defined. Table 3 shows the normal target thickness (mm) that can be perforated as a function of obliquity and range (or velocity). A muzzle velocity of 1,800 m/s and an aerodynamic retardation in velocity of 267 m/s/km were used in the analysis.

All of the terminal effects are incorporated in Table 3. At 0° obliquity, the penetration at muzzle velocity (1,800 m/s) is very high (74.2 mm) and drops rapidly (36.2 mm) at extended range, 2,000 m (1,260 m/s) As obliquity is increased at the muzzle velocity, the LOS thickness capability is drastically decreasing, going from 74.2 mm at 0° to 60 mm (30 mm normal) at 60°, and 53 mm (18.1 mm normal) at 70°. At the 2,000-m range, however, the LOS thickness is fairly constant, ranging from 36.2 mm at 0° to 36.8 mm (18.4 mm normal) at 60°, and 36.5 mm (12.5 mm normal) at 70°. Finally, at the lowest velocities (1,132 m/s) or extreme range (2,500 m), the obliquity effect is slightly reversed. At 0° it will perforate 28.8 mm, at 60° the LOS thickness is 30.2 mm (15.1 mm normal), and at 70° it is 30.4 mm (10.4 mm normal). There is not sufficient data at much lower velocities to comment on the trend for even thinner targets.

Table 3. Estimated Normal Perforation Thickness (mm) for the 0.60-cal. APFSDA Against RHA

Obliquity (°)	Range (m)								
	0	500	750	1,000	1,250	1,500	1,750	2,000	2,500
0	74.2	63.5	58.4	53.5	48.9	44.5	40.2	36.2	28.8
5	73.9	63.2	58.1	53.3	48.7	44.3	40.1	36.1	28.7
10	72.8	62.3	57.3	52.6	48.0	43.8	39.6	35.7	28.4
15	71.0	60.9	56.1	51.4	47.0	42.9	38.9	35.0	27.9
20	68.5	58.8	54.3	49.9	45.6	41.6	37.8	34.1	27.2
25	65.3	56.3	52.0	47.8	43.9	40.1	36.4	32.9	26.3
30	61.6	53.3	49.3	45.4	41.7	38.2	34.8	31.5	25.2
35	57.3	49.8	46.2	42.6	39.3	36.0	32.9	29.8	23.9
40	52.5	45.9	42.6	39.5	36.5	33.6	30.7	27.9	22.5
45	47.3	41.6	38.8	36.1	33.4	30.8	28.3	25.8	20.9
50	41.8	37.0	34.7	32.4	30.1	27.9	25.7	23.6	19.1
55	36.0	32.2	30.3	28.4	26.6	24.7	22.9	21.1	17.2
57	33.7	30.2	28.5	26.8	25.1	23.4	21.7	20.0	16.4
60	30.0	27.2	25.7	24.3	22.8	21.3	19.9	18.4	15.1
62	27.6	25.1	23.8	22.5	21.2	19.9	18.6	17.3	14.2
65	24.0	22.0	21.0	19.9	18.8	17.8	16.6	15.5	12.8
67	21.6	19.9	19.1	18.2	17.2	16.3	15.3	14.3	11.9
70	18.1	16.9	16.2	15.5	14.8	14.1	13.3	12.5	10.4
72	15.8	14.8	14.3	13.8	13.2	12.6	12.0	11.3	9.4
Velocity (m/s)	1,800	1,667	1,600	1,533	1,466	1,400	1,333	1,266	1,132

The perforation data at 0° obliquity and 1,500-m range compare favorably with the semi-infinite, APFSDA design results (approximately 45 mm) from open literature data (Zielinski 1991). Of course, prediction of the obliquity effects was not possible from the reference.

For lack of data, similar derivations were not constructed for the HHA. It is obvious, however, that a large obliquity effect prevails, as the gap between the two limit velocities is much greater than that for the corresponding RHA. This by itself shows how it is not possible to extrapolate from RHA to HHA with this limited data set. Because only one thickness for each obliquity was evaluated, the dependence with respect to thickness could not be determined either.

8. CONCLUSIONS

A terminal ballistic evaluation of a TBS for a candidate electromagnetically launched 0.60-cal. APFSDA projectile into RHA was completed. By applying the launch and flight characteristics of the design projectile, estimates for its defeat ranges were developed.

The intricate design of the actual EM projectile was simulated by an equal length and diameter right circular cylinder with the same conical nose shape. The conical nose design proved detrimental at the higher obliquity. At high velocities, the performance into 0° RHA was quite good. At these higher velocities and thicker armor plates, however, the performance at obliquity dropped drastically. For extended ranges or lower impact velocity, the perforation at 0° and the LOS thickness at obliquity is respectable.

Two HHA targets were also evaluated and tabulated for future reference. It was noted that the extremely small-diameter rod did not contribute to the plugging as much as might be expected for similar caliber armor-piercing (AP) rounds. The main portion of defeating thin HHA plates is usually the plugging phase. It would be possible to refine the TBS design by incorporating the performance of an HHA target in the methodology. In contrast, for the RHA, where most of the perforation process is penetration, the 0.60-cal. TBS has comparable performance.

9. REFERENCES

Farrand, T. G., and J. A. Zook. "A Compilation of Nose Shape and Obliquity Test into Semi-infinite Targets." Memo for Alex Zielinski. U.S. Army Research Laboratory, Aberdeen Proving Ground, MD, December 1992.

Grabarek, C. L. "Penetration of Armor by Steel and High Density Penetrators." (AD 518394L) BRL-MR-2134, U.S. Army Ballistic Research Laboratory, Aberdeen Proving Ground, MD, October 1971.

Grabarek, C. L., and E. L. Herr. "X-Ray Multi-Flash System for Measurement of Projectile Performance at the Target." BRL-TN-1634, U.S. Army Research Laboratory, Aberdeen Proving Ground, MD, September 1966.

Kitzmiller, J., R. W. Faidley, R. L. Fuller, G. R. Headifen, S. B. Pratal, M. L. Spann, and R. F. Thelen. "Final Design at an Air Core, Compulsator Driver, 60-Caliber Railgun System." IEEE Transactions on Magnetics, vol. 27, no. 1, January 1991.

Lambert, J. P., and G. H. Jonas. "Towards Standardization in Terminal Ballistic Testing: Velocity Representation." BRL Report 1852, U.S. Army Ballistic Research Laboratory, Aberdeen Proving Ground, MD, January 1976.

Magness, L. S., T. G. Farrand, N. L. Van Rensselear, and C. L. Grabarek. "An Evaluation of Candidate Tungsten, Tungsten Carbide, and Depleted Uranium Alloys for the XM903 Caliber 0.50 Saboted Light Armor Penetrator (SLAP) Round." BRL-MR-3702, U.S. Army Ballistic Research Laboratory, Aberdeen Proving Ground, MD, November 1988.

Silsby, G. F., R. Roszak, and L.-Giglio Tos. "BRL's 50-mm High Pressure Powder Gun for Terminal Ballistic Testing - The First Year's Experience." BRL-MR-03236, U.S. Army Ballistic Research Laboratory, Aberdeen Proving Ground, MD, January 1983.

Zielinski, A. E. "Design Limitations for Small Caliber Electromagnetic Saboted Rod Projectiles." IEEE Transactions on Magnetics, vol. 27, no. 1, January 1991.

INTENTIONALLY LEFT BLANK.

APPENDIX A:

AN EXPLANATION OF FIGURES AND TABLES OF INDIVIDUAL FIRING DATA

INTENTIONALLY LEFT BLANK.

The following is a description of the table headings and columns which are used in the individual shot data for each test series detailed in Appendix B.

The "test series label" at the top of each table describes the particular configuration common to the firings listed below the heading. Each "test series table" is organized into three subtables. The uppermost subtable, essentially a "black-box" description, lists the most important measurable preimpact parameters, such as the striking velocity, mass, yaw, and pitch, followed by the most important post-impact data, including the residual penetrator's mass, velocity, and flight direction. A negative shot number indicates that the resulting data was not considered a "fair hit" and, therefore, not used in the limit velocity or V-50 determination.

The other two subtables tabulate additional post-impact data such as the target plug mass and velocity; the entrance, exit, and midplate dimensions of the perforation hole; and other behind-armor debris measures for single plate targets. Figures A-1 through A-4 illustrate many of the measurable quantities for single plate targets. For the spaced array target, Figure A-5 depicts the measured parameters unique to spaced plate targets.

An additional set of data, generated to determine characteristics of penetration into semi-infinite armor, is also included in the following appendix. The values listed in this table are obtained by sectioning the semi-infinite plate along the centerline of the penetration hole. This table is divided into two subtables, the first is the "black-box" table, and the other contains secondary measures of the penetration tunnel. Figure A-6 is a schematic of the sectioned penetration tunnel and its related measures.

Below is an alphabetical listing of the abbreviations used as column headings in each of the subtables, with a definition of each term and a brief description of how it is measured. Also included are some of the abbreviations used for the entries in the columns. Some of the listings below may not have entries in the test series tables generated as part of this report.

A - an adjustable parameter in the limit velocity functional formulation, $Vr = A\,(Vs^p - Vl^p)^{1/p}$, where A is the slope of the asymptote of the fitted curve, restricted to $A<1$.

α - the striking pitch, orientation of the projectile relative to its flight path, measured in the vertical plane, degrees (see Figure A-1).

$\alpha 1$ ($\alpha 2$) - pitch of projectile after perforating the first (second) plate of spaced array target, relative to projectile's flight path, degrees (see Figure A-5).

αR - the pitch of final residual penetrator, relative to its residual flight path; the entry NA appears if the residual penetrator is tumbling rapidly, degrees (see Figure A-1).

Area - the cross-sectional area of the penetrator, used for comparisons in the semi-infinite data, square centimeters.

Area hole - the average cross-sectional area of the hole produced in semi-infinite test, measured by using the diameter of the sectioned armor and assuming a circular tunnel, square centimeters (see Figure A-6).

β - the striking yaw, orientation of the projectile relative to its flight path, measured in the horizontal plane, degrees.

BG/L or Blg. - height of lip on the exit hole or bulge height, height above the rear surface of the plate, measured perpendicular to surface, centimeters (see Figures A-2, A-3).

BHN - Brinell Hardness of monolithic target plate.

BHN1, BHN2, BHN3 - Brinell Hardness of first, second, and third plates of spaced array target.

BlgL - bulge length, length of rear surface bulge of finite monolithic target or of last plate in spaced array target, centimeters (see Figure A-2).

BlgW - bulge width, width of rear surface bulge of finite monolithic target or of last plate in spaced array target, centimeters.

CenL - center hole length, length of penetration hole at midthickness in the plate, measured in the plane of target, centimeters (see Figure A-3).

CenW - center hole width, width of penetration hole at midthickness in the plate, centimeters (see Figure A-3).

CL PL#1,2,3 - center hole length in first (second, third) plate of spaced array target, length of penetration hole at midthickness in the plate, centimeters.

CW PL#1,2,3 - center hole width in first (second, third) plate of spaced array target, width of penetration hole at midthickness in the plate, centimeters.

CoFS - center of fragment spray angle, the average direction of the behind-armor debris, measured relative to the penetrator's original flight path, estimated from the behind-armor radiographs in the vertical plane, degrees (see Figure A-4).

Cone - cone angle or enclosed spray angle, angle in space which encloses the behind-armor debris cloud, estimated from behind-armor radiographs in the vertical plane, degrees (see Figure A-4).

Dt/Dp - Diameter of the tunnel produced in semi-infinite targets divided by the original diameter of the penetrator, nondimensional.

EHL - exit hole length, length of exit hole on rear surface of plate, measured in plane of plate, centimeters (see Figure A-3).

EHW - exit hole width, width of exit hole on rear surface of plate, measured in plane of plate, centimeters (see Figure A-3).

EntHL - entrance hole length, length of entrance hole on front surface of target, measured in plane of target plate, centimeters (see Figure A-3).

EntW - entrance hole width, width of entrance hole on front surface of target, measured in plane of target plate, centimeters (see Figure A-3).

ηp - departure angle of target plug, measured relative to penetrator's original flight path, from x-ray images in the vertical plane, degrees (see Figure A-1).

$\eta 1$ ($\eta 2$, $\eta 3$) - departure angle of residual penetrator after exiting the first (second, third) plate of a spaced array target, measured relative to penetrator's original flight p h, from x-ray images in the vertical plane, degrees (see Figure A-5).

F - fineness ratio, the length-to-diameter (L/D) ratio of the penetrator.

γ - total solid angle orientation of the striking penetrator to its initial flight path ($\alpha^2 + \beta^2 = \gamma^2$), degrees.

K.E. - kinetic energy, the kinetic energy of the round impacting the semi-infinite target, joules.

KE/A - kinetic energy divided by cross-sectional area of penetrator, the energy per area impacting semi-infinite armor, joules/square centimeter.

KE/Vt - kinetic energy divided by total volume, the energy impacting the armor divided by the total volume of the tunnel generated while penetrating semi-infinite armor, joules/cubic centimeter.

LP - length of target plug, average dimension of plug, oriented to correspond to exit hole length in target, where applicable, used in residual plug mass estimates, centimeters.

M/A - mass of penetrator divided by cross-sectional area of penetrator, used primarily in semi-infinite data, grams/square centimeter.

M/A hole - mass of penetrator divided by cross-sectional area of hole generated in semi-infinite penetration, grams/square centimeter.

MPL - mass of target plug or plugs, estimated from behind-armor radiographic images, grams (see Figure A-1).

MPr - recovered plug mass or masses, actual mass of plug recovered after a test firing, compared with MPL value as a check on estimation accuracy, grams.

Mr - mass of residual penetrator or residual penetrators, estimated from images in behind-armor radiographs, grams (see Figure A-1).

MR1 (2) - residual mass of penetrator after perforating the first (second) plate of a spaced array target, estimated from radiographic images, grams (see Figure A-5).

M.R. Dia - maximum rod diameter, maximum diameter of the mushroomed portion of the final residual penetrator, if applicable, centimeters.

M. rec - mass of recovered residual penetrator, compared with Mr values as a check on estimation accuracy, grams.

Ms - mass of penetrator before target impact, grams (see Figure A-1).

NC - not calculated.

NM - not measured.

NR - not recovered.

No. of Pcs. - number of major identifiable final residual penetrator pieces seen in behind-armor radiographic images. The breakup behavior of the penetrator is indicated by a number code:

1 - one whole piece
21 - two pieces, fracture at nose section
22 - two pieces, fracture at tail section
23 - two pieces, fracture at midlength
31 - three pieces, fracture at nose section
32 - three pieces, fracture at tail section
33 - three pieces, evenly distributed fractures
Frag - many pieces, too small to accurately measure.

#Pc1 (2) - number of major residual penetrator pieces after first (second) plate of spaced array target, uses same number code as No. of Pcs. on previous page, with addition of 40 - four or more pieces.

P - an adjustable parameter of the limit velocity determination equation $Vr = A\,(Vs^P - Vl^P)\frac{1}{P}$, where P is the power determining how rapidly the fitted curve rises to the asymptote, arbitrarily restricted to $1 < P < 8$ values.

Pen., Pene or Pn- penetration depth into target plate (finite, semi-infinite, or last plate of spaced array target), for partial penetrations measured normal to the plate surface, centimeters (see Figure A-2 and A-6).

P/L - penetration depth divided by original length of penetrator, nondimensional term used in normalizing the depth of penetration into semi-infinite armor.

ρlv^2 - density times the length times the velocity squared of the penetrator, a term used to characterize the impacting penetrator into a semi-infinite plate, grams/square second.

Rise - target plate rise, rise of the front surface of the target plate encountered after the penetrator has impacted the semi-infinite armor, centimeters (see Figure A-6).

Rot - rotation, the apparent change in pitch of the final residual penetrator between the two behind-armor x-ray images, indicative of penetrator tumbling, degrees.

RotR 1 (2) - rotation rate (pitch rate) of the residual penetrator after the first (second) plate of spaced array target, using the convention that rotation of the nose of the rod toward the target normal is positive, degrees/second (see Figure A-5).

S - standard deviation, measure of the data spread of Vs, Vr data pairs from the fitted Vs-Vr curve, measured on the Vr axis (vertical) only, meters/second.

Shot No. or Sh.# - shot number, the individual test firing identification number; a negative number indicates that the resulting data was not considered a "fair hit" and, therefore, not used in the limit velocity or V-50 determination.

Time - time between the two behind-armor x-ray flashes, microseconds.

Th. - target plug thickness, the thickness of the rear surface of the target plate that was removed as a plug, estimated from x-ray images of the target plug, used in plug mass estimates, centimeters.

Vol Base (Tot) - volume of the penetration hole within target (total volume of penetration tunnel, including portion created from Rise), estimated volume of the penetration tunnel created in semi-infinite armor, determined by estimating area of half section and assuming the tunnel was circular, cubic centimeters (see Figure A-6).

Vpl - velocity of the target plug, as measured in the vertical plane, calculated from behind-armor radiographic images, meters/second (see Figure A-1).

Vr - velocity of the final residual penetrator, measured in the vertical plane, calculated from behind-armor radiographic images, meters/second (see Figure A-1).

Vr1 (2) - velocity of the residual penetrator after the first (second) plate of spaced array target, meters/second (see Figure A-5).

Vs - striking velocity of penetrator, calculated from preimpact images of penetrator in both vertical and horizontal planes, meters/second (see Figure A-1).

W.p - width of target plug, average dimension of plug, oriented to correspond to exit hole width in target plate where applicable, estimated from x-ray images of target plug, used in plug mass estimates, centimeters.

Wt. L - net weight loss of target plate, determined by measuring weight of target plate before and after each test firing, grams.

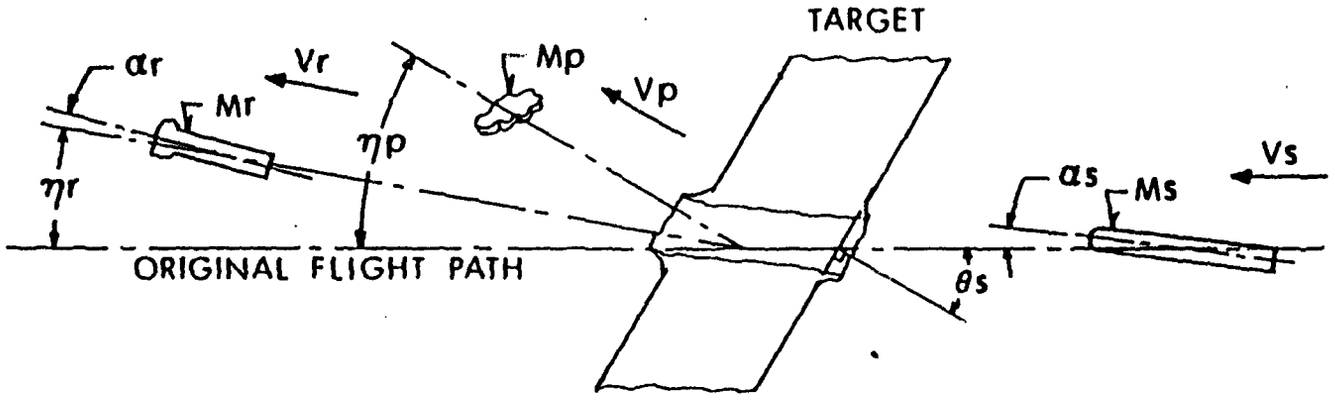

RESIDUAL PENETRATOR
Vr = VELOCITY, m/s
Mr = MASS, GRAMS
αr = INDUCED PITCH, DEGREES
ηr = INDUCED FLIGHT PATH, DEGREES

PLUG
Vp = VELOCITY, m/s
Mp = MASS, GRAMS
ηp = DEPARTURE, DEGREES

STRIKING
Vs = VELOCITY, m/s
Ms = MASS, GRAMS
αs = PITCH, DEGREES
θs = OBLIQUITY, DEGREES

Figure A-1. Illustration of primary preimpact and postimpact radiographic measures.

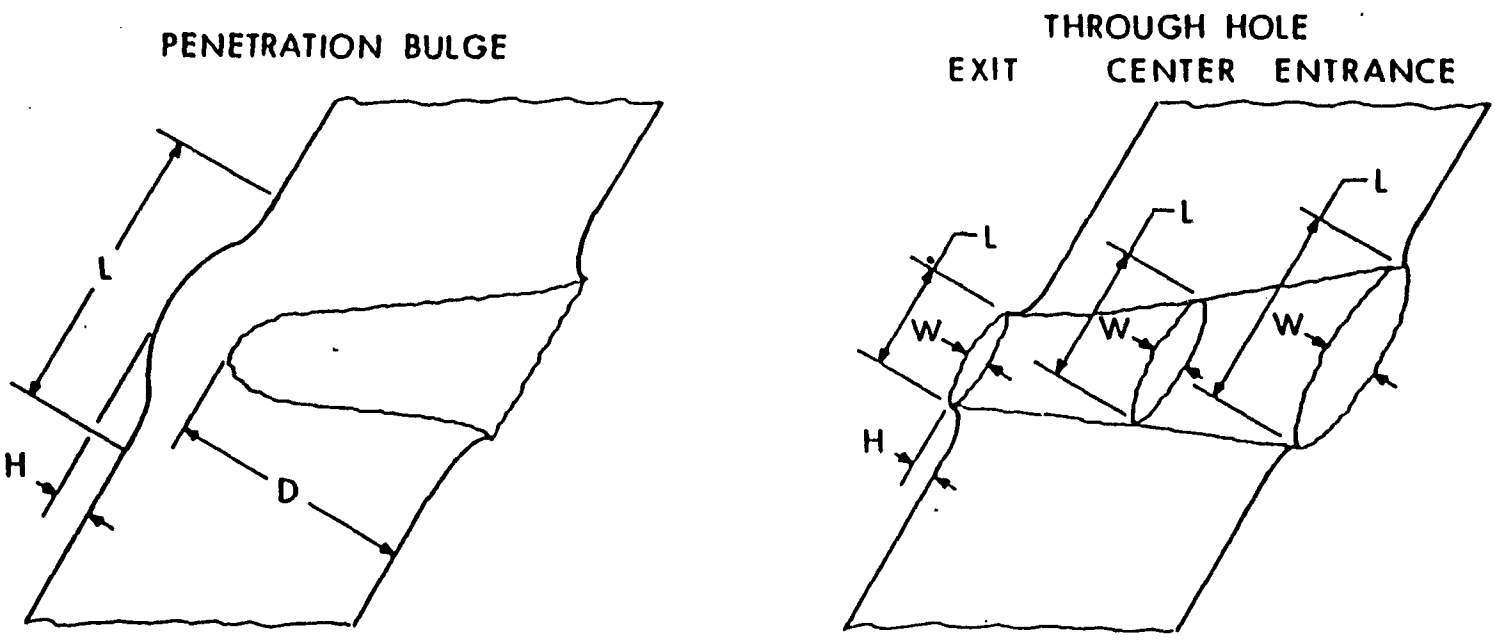

Figure A-2. Illustration of target plate measures - partial penetration.

Figure A-3. Illustration of target plate measures - complete penetration.

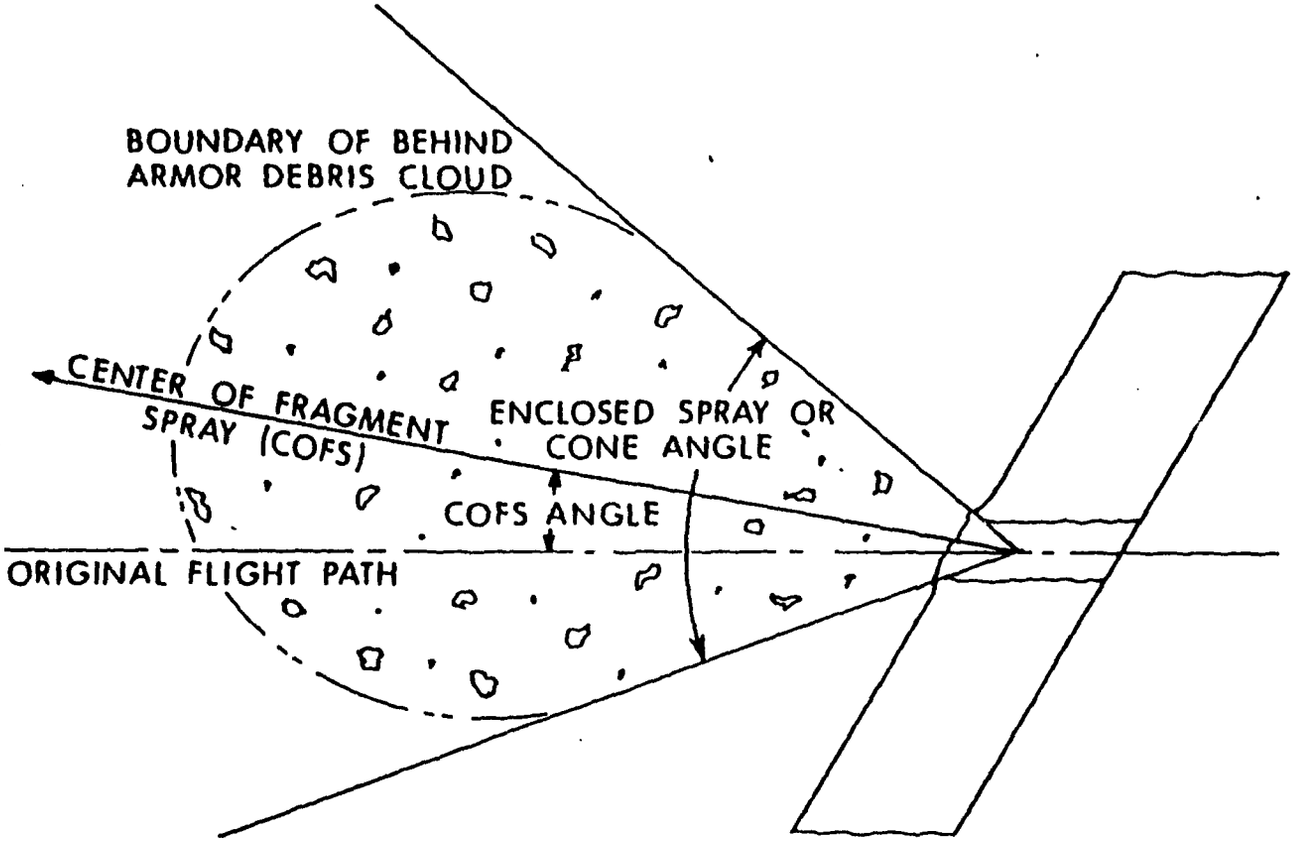

Figure A-4. Illustration of radiographic behind-armor debris measures.

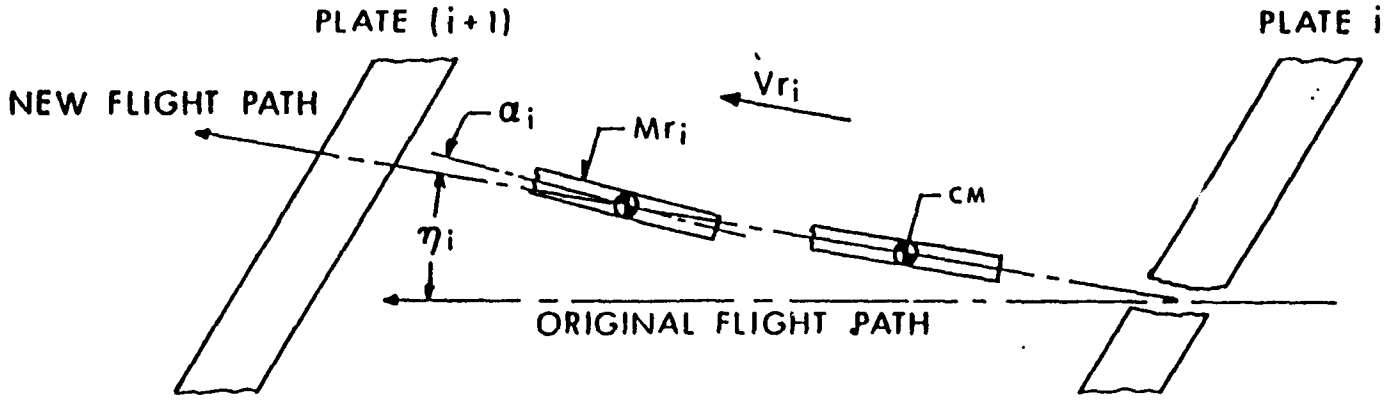

Figure A-5. Illustration of between-plate measures in spaced array target.

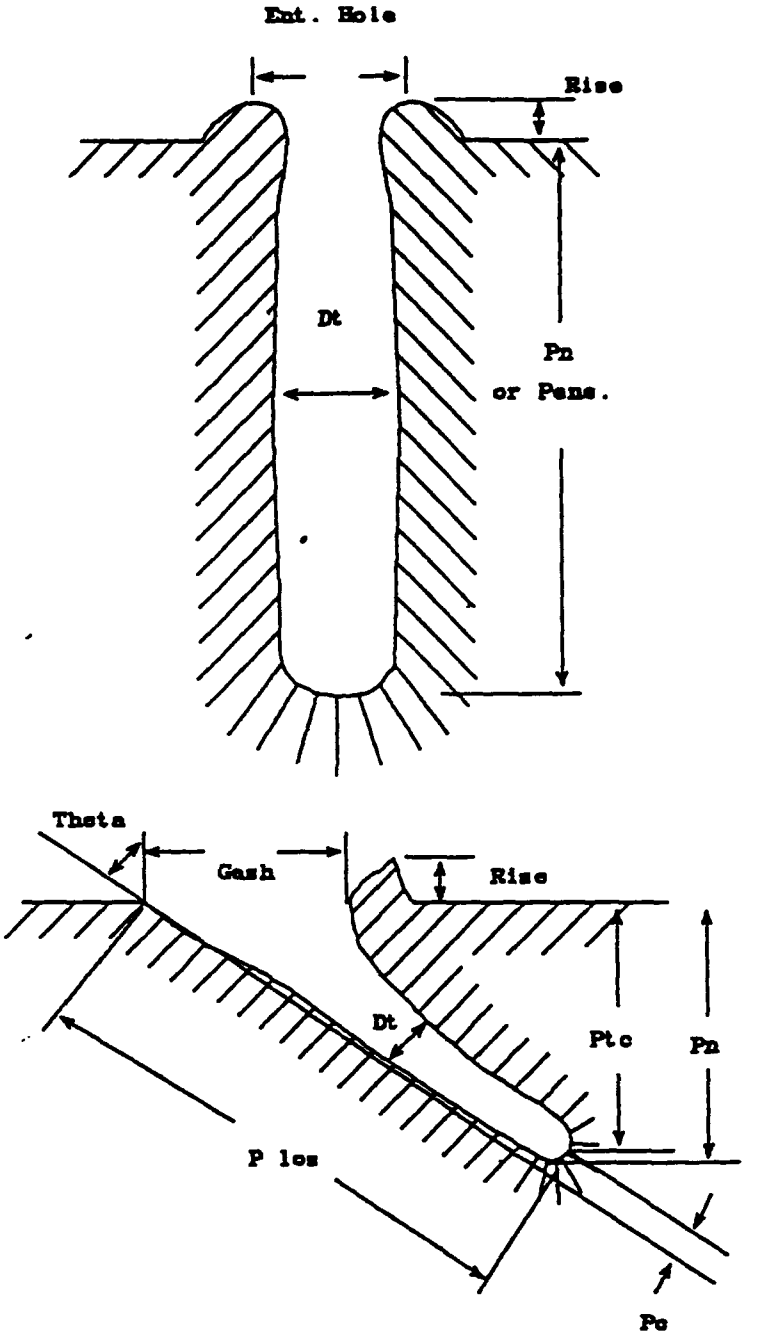

Figure A-6. Illustration of penetration measures in semi-infinite target.

APPENDIX B:

TABULATIONS OF INDIVIDUAL SHOT DATA

INTENTIONALLY LEFT BLANK.

Table B-1. Individual Shot Data Tabulation for the 0.60-cal. TBS Against Semi-Infinite RHA at 0° Obliquity

Series Fired 3 - 1992
L/D = 15, Density is 17.6

Shot No.	γ (°)	V_s (m/s)	M_s (g)	K.E. (J)	Area (cm^2)	M/A (g/cm^2)	KE/A (J/cm^2)	Normal P/L	Normal Penetration (mm)
1136	1.27	1,220	12.82	9,541	0.122	105	78,371	0.45	30.0
1137	1.46	1,122	12.81	8,063	0.122	105	66,234	0.40	26.2
1138	0.75	1,260	12.83	10,184	0.122	105	83,660	0.51	33.8
1139	2.30	1,490	12.81	14,220	0.122	105	116,808	0.68	45.2
1140	0.90	1,699	12.81	18,489	0.122	105	151,875	0.99	65.5
1141	0.79	1,861	12.76	22,096	0.122	105	181,507	1.15	75.7
1142	2.02	1,485	12.77	14,080	0.122	105	115,663	0.74	49.0

Table B-1. Individual Shot Data Tabulation for the 0.60-cal. TBS Against Semi-Infinite RHA at 0° Obliquity (continued)

Series Fired 3 - 1992
L/D = 15, Density is 17.6

Shot No.	Rise (cm)	Volume Base (cm^3)	Volume Total (cm^3)	KE/Vt (J/cm^3)	KE/Vb (J/cm^3)	ρ/v^2 *10^6	Dt/Dp	Area Hole (cm^2)	M/A Hole (g/cm^2)
1136	0.00 BHN = 302	0.72	0.72	13,251	13,251	173	1.78	0.38	33.31
1137	0.00 BHN = 302	1.78	1.78	4,530	4,530	147	1.78	0.38	33.29
1138	0.00 BHN = 302	2.15	2.15	4,737	4,737	185	1.78	0.38	33.34
1139	0.00 BHN = 302	1.34	1.34	10,612	10,612	258	1.52	0.28	45.31
1140	0.00 BHN = 302	2.63	2.63	7,030	7,030	336	1.52	0.28	45.31
1141	0.00 BHN = 286	4.86	4.86	4,546	4,546	400	1.78	0.38	33.16
1142	0.00 BHN = 286	1.35	1.35	10,430	10,430	257	1.52	0.28	45.16

Table B-2. Individual Shot Data Tabulation for the 0.60-cal. TBS Against 50.8-mm RHA at 0° Obliquity

Series Fired 3 - 1992
Limit Velocity = 1,483, A = .96, P = 4.09, S = 4

Shot No.	α (°)	β (°)	γ (°)	V_s (m/s)	M_s (g)	η_R (°)	α_R (°)	V_r (m/s)	M_r (g)	Pen. (cm)
1143	0.00	0.50L	0.50	1,342	12.91	NA	NA	0	0.00	NM
1144	1.25D	0.75L	1.46	1,347	12.81	NA	NA	0	0.00	NM
1145	0.25U	0.00	0.25	1,369	12.83	NA	NA	0	0.00	NM
1146	2.00D	1.50R	2.50	1,409	12.76	NA	NA	0	0.00	NM
1147	0.50U	0.50L	0.71	1,666	12.85	1.6U	NA	1,313 1,300	1.94 1.82	CP
1148	0.50D	0.75R	0.90	1,512	12.78	0.2U	NA	794	1.82	CP
1149	1.25U	1.25R	1.77	1,454	12.81	NA	NA	0	0.00	NM
1150	0.50U	0.25L	0.56	1,494	12.81	0.4U	NA	636	1.57	CP

Table B-2. Individual Shot Data Tabulation for the 0.60-cal. TBS Against 50.8-mm RHA at 0° Obliquity (continued)

Series Fired 3 - 1992
Limit Velocity = 1,483, A = .96, P = 4.09, S = 4

Shot No.	M.rec (g)	η_P (°)	V_{pl} (m/s)	M_{pl} (g)	M_{pr} (g)	L.p (cm)	W.p (cm)	Th. (cm)	EHL (cm)	EHW (cm)	Blg (cm)	Wt.L (g)
1143	0.00 BHN = 321	NA	0	0.00	0.00	0.0	0.0	0.0	0.0	0.0	0.2	33
1144	0.00 BHN = 321	NA	0	0.00	0.00	0.0	0.0	0.0	0.0	0.0	0.2	5
1145	0.00 BHN = 321	NA	0	0.00	0.00	0.0	0.0	0.0	0.0	0.0	0.3	-1
1146	0.00 BHN = 321	NA	0	0.00	0.00	0.0	0.0	0.0	0.0	0.0	0.1	-106
1147	0.00 BHN = 321	0.0	0	0.00	0.00	0.0	0.0	0.0	1.4	1.5	NR	13
1148	0.00 BHN = 321	NM	LOST	LOST	NONE	NM	NM	NM	1.1	1.1	NR	10
1149	0.00 BHN = 321	NA	0	0.00	0.00	0.0	0.0	0.0	0.0	0.0	0.5	9
1150	0.00 BHN = 321	Spall - Fragments							0.0	0.0	0.6	33

Table B-2. Individual Shot Data Tabulation for the 0.60-cal. TBS Against 50.8-mm RHA at 0° Obliquity (continued)

Series Fired 3 - 1992
Limit Velocity = 1,483, A = .96, P = 4.09, S = 4

Shot No.	Cone (°)	CoFS (°)	EntHL (cm)	EntW (cm)	CenL (cm)	CenW (cm)	No. Pcs.	M.R. Dia. (in)	BL (cm)	BW (cm)
1143	NA	NA	1.1	1.1	0.9	0.9	PP	PP	2.5	2.5
1144	NA	NA	1.1	1.1	0.9	0.8	PP	PP	2.7	2.5
1145	NA	NA	1.1	1.1	0.7	0.8	PP	PP	2.6	2.5
1146	NA	NA	1.0	1.0	0.7	0.7	PP	PP	2.6	2.6
1147	1.0	1.2U	1.0	0.9	0.9	0.9	2	NM	NM	NM
1148	0.0	0.2U	1.1	1.0	0.5	0.5	1	NM	NM	NM
1149	NA	NA	1.0	1.0	0.7	0.7	PP	PP	2.3	2.5
1150	0.0	0.4U	1.0	1.0	0.6	0.7	1	PP	1.2	1.1

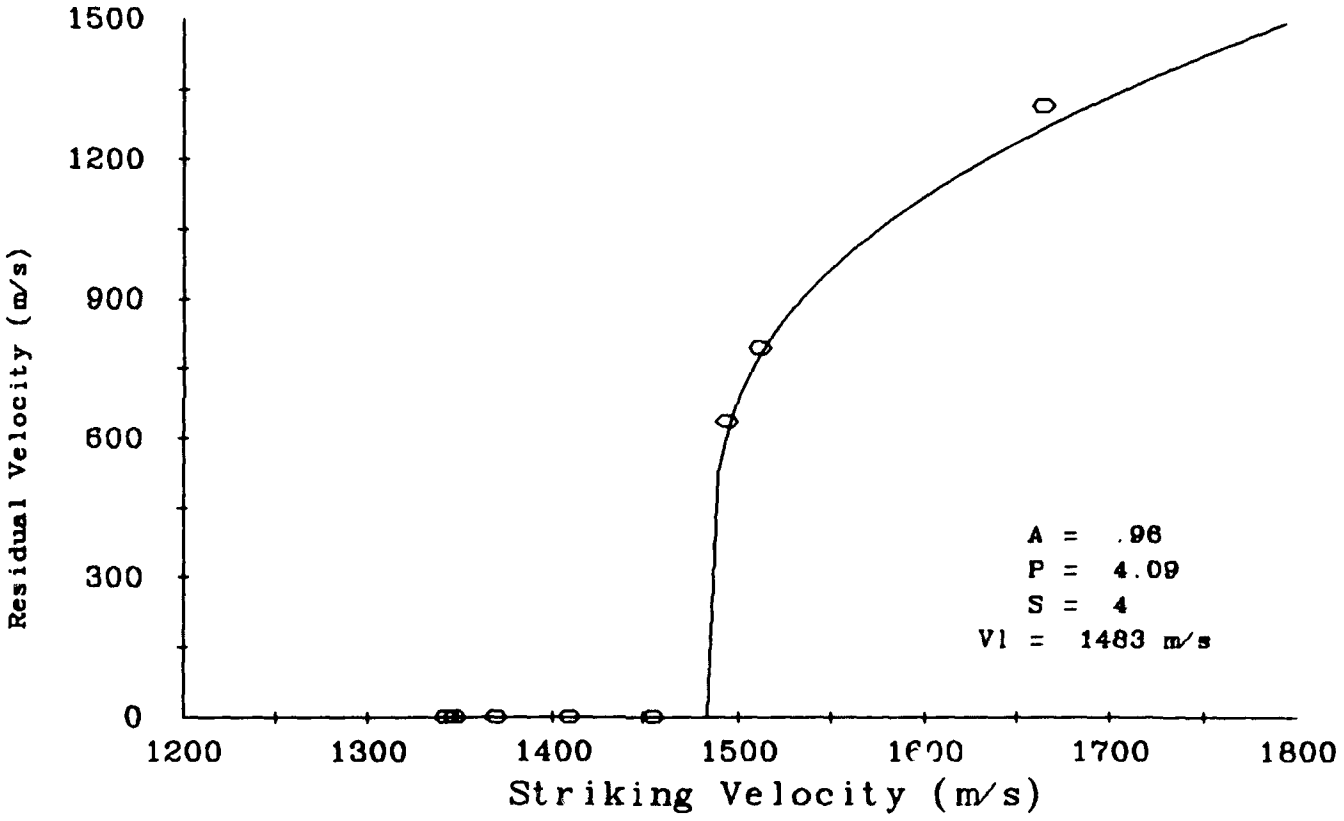

Figure B-1. V_o-V_r curve for the 0.60-cal. TBS against 50.8-mm-RHA at 0° obliquity.

Table B-3. Individual Shot Data Tabulation for the 0.60-cal. TBS Against 19.05-mm RHA at 57° Obliquity

Series Fired 3 - 1992
Limit Velocity = 1,220, A = 1, P = 3.29, S = 133

Shot No.	α (°)	β (°)	γ (°)	V_s (m/s)	M_s (g)	η_R (°)	α_R (°)	Vr (m/s)	Mr (g)	Pen. (cm)
1152	1.25U	0.75R	1.46	1,306	12.78	7.9U	NA	958	2.81	CP
1153	0.00	0.25L	0.25	1,265	12.80	18.7U	NA	627	1.24	CP
1154	1.50U	0.75R	1.67	1,241	12.79	16.9U	NA	723	1.90	CP
1155	0.00	0.25R	0.25	1,186	12.82	NA	NA	0	0.00	1.2
1156	2.25D	1.00R	2.46	1,212	12.78	NA	NA	0	0.00	0.6
1157	1.25D	2.25L	2.57	1,220	12.80	NA	NA	0	0.00	0.7
1158	1.50U	0.25L	1.52	1,243	12.72	12.4U	NA	794	1.94	CP
1159	0.00	0.75R	0.75	1,221	12.83	58.7U	NA	142	0.80	CP

Table B-3. Individual Shot Data Tabulation for the 0.60-cal. TBS Against 19.05-mm RHA at 57° Obliquity (continued)

Series Fired 3 - 1992
Limit Velocity = 1,220, A = 1, P = 3.29, S = 133

Shot No.	M.rec (g)	η_p (°)	V_{pl} (m/s)	M_{pl} (g)	M_{pr} (g)	L.p (cm)	W.p (cm)	Th. (cm)	EHL (cm)	EHW (cm)	Blg (cm)	Wt.L (g)
1152	0.00 BHN = 340	NM	Lost	Lost	None	NM	NM	NM	1.7	1.4	NR	8
1153	0.00 BHN = 340	NM	Lost	Lost	None	NM	NM	NM	1.5	1.3	NR	15
1154	0.00 BHN = 346	31.6U	719	2.28	0.00	0.8	0.6	0.6	1.5	1.2	NR	9
1155	0.00 BHN = 364	NA	0	0.00	0.00	0.0	0.0	0.0	0.0	0.0	0.1	14
1156	0.00 BHN = 364	NA	0	0.00	0.00	0.0	0.0	0.0	0.0	0.0	0.1	9
1157	0.00 BHN = 364	NA	0	0.00	0.00	0.0	0.0	0.0	0.0	0.0	0.0	19
1158	0.00 BHN = 364	25.8U	721	1.74	0.00	0.8	0.5	0.5	0.5	1.0	NR	9
1159	0.00 BHN = 364	68.8U	130	3.95	0.00	0.9	0.7	0.7	0.9	0.9	NR	9

Table B-3. Individual Shot Data Tabulation for the 0.60-cal. TBS Against 19.05-mm RHA at 57° Obliquity (continued)

Series Fired 3 - 1992
Limit Velocity = 1,220, A = 1, P = 3.29, S = 133

Shot No.	Cone (°)	CoFS (	EntHL (cm)	EntW (cm)	CenL (cm)	CenW (cm)	No. Pcs.	M.R. Dia. (in)	BL (cm)	BW (cm)
1152	0.0	7.9U	1.5	0.5	0.7	0.7	1	NM	NM	NM
1153	8.5	22.9U	2.3	0.8	0.8	0.6	2	NM	NM	NM
1154	14.7	24.3U	1.8	0.8	0.7	0.6	2	NM	NM	NM
1155	NA	NA	3.5	0.8	0.0	0.0	PP	PP	2.1	1.2
1156	NA	NA	4.1	1.1	0.8	2.1	PP	PP	NM	NM
1157	NA	NA	0.7	5.0	0.8	2.5	PP	PP	0.0	0.0
1158	13.4	19.1U	0.8	0.5	0.9	0.5	2	NM	NM	NM
1159	10.1	63.8U	2.5	0.5	0.5	0.5	2	NM	NM	NM

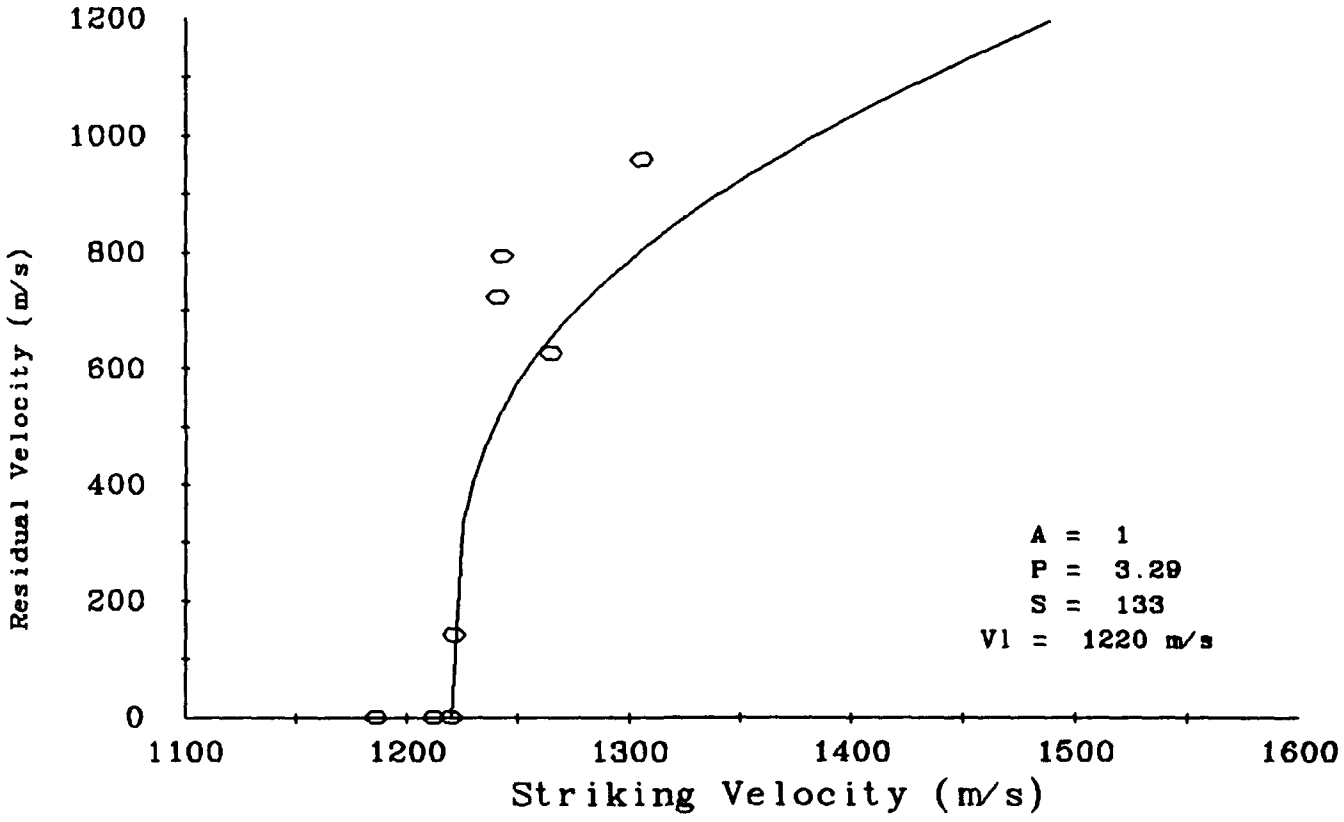

Figure B-2. V_c-V_r curve for the 0.60-cal. TBS against 19.05-mm RHA at 57° obliquity.

Table B-4. Individual Shot Data Tabulation for the 0.60-cal. TBS Against 31.75-mm RHA at 57° Obliquity

Series Fired 3 - 1992
Limit Velocity = 1,716, A = .95, P = 6.89, S = 0

Shot No.	α (°)	β (°)	γ (°)	V_s (m/s)	M_s (g)	η_R (°)	α_R (°)	V_r (m/s)	M_r (g)	Pen. (cm)
1160	0.50U	0.50L	0.70	1,357	12.81	NA	NA	0	0.00	NM
1161	0.25D	0.00	0.25	1,510	12.73	NA	NA	0	0.00	2.5
1162	0.75D	0.00	0.75	1,610	12.77	NA	NA	0	0.00	NM
-1163	1.00U	0.25R	1.02	1,777	12.78	NA	NA	Lost	Lost	CP
1164	0.75D	0.00	0.75	1,696	12.84	NA	NA	0	0.00	1.3
1165	0.00	0.25L	0.25	1,760	12.71	3.1U	NA	1309	1.86	CP
1166	0.50D	1.25R	1.35	1,217	12.77	NA	NA	0	0.00	0.5
1167	0.25U	0.50L	0.56	1,730	12.72	6.2U	NA	1100	1.24	CP

Table B-4. Individual Shot Data Tabulation for the 0.60-cal. TBS Against 31.75-mm RHA at 57° Obliquity (continued)

Series Fired 3 - 1992
Limit Velocity = 1,716, A = .95, P = 6.89, S = 0

Shot No.	M.rec (g)	η_P (°)	V_{pl} (m/s)	M_{pl} (g)	M_{pr} (g)	L.p (cm)	W.p (cm)	Th. (cm)	EHL (cm)	EHW (cm)	Blg (cm)	Wt.L (g)
1160	0.00 BHN = 340	NA	0	0.00	0.00	0.0	0.0	0.0	0.0	0.0	0.1	4
1161	0.00 BHN = 340	NA	0	0.00	0.00	0.0	0.0	0.0	0.0	0.0	0.2	5
1162	0.00 BHN = 340	NA	0	0.00	0.00	0.0	0.0	0.0	0.0	0.0	0.1	2
-1163	None BHN = 340	Lost	Lost	Lost	None	NM	NM	NM	2.0	1.5	0.0	24
1164	0.00 BHN = 321	NA	0	0.00	0.00	0.0	0.0	0.0	0.0	0.0	0.1	16
1165	0.00 BHN = 321	Spall - Fragments							1.9	1.5	NR	32
1166	0.00 BHN = 321	NA	0	0.00	0.00	0.0	0.0	0.0	0.0	0.0	0.0	55
1167	0.00 BHN = 321	NM	Lost	Lost	None	NM	NM	NM	1.8	1.2	NR	7

Table B-4. Individual Shot Data Tabulation for the 0.60-cal. TBS Against 31.75-mm RHA at 57° Obliquity (continued)

Series Fired 3 - 1992
Limit Velocity = 1,716, A = .95, P = 6.89, S = 0

Shot No.	Cone (°)	CoFS (°)	EntHL (cm)	EntW (cm)	CenL (cm)	CenW (cm)	No. Pcs.	M.R. Dia. (in)	BL (cm)	BW (cm)
1160	NA	NA	1.5	0.7	0.7	0.8	PP	PP	1.7	1.8
1161	NA	NA	1.7	0.4	0.7	0.8	PP	PP	1.7	1.5
1162	NA	NA	2.5	0.6	0.7	0.7	PP	PP	3.1	2.0
-1163	Lost	Lost	2.3	0.7	1.0	0.9	Lost	Lost	0.0	0.0
1164	NA	NA	2.7	0.7	0.0	NM	PP	PP	3.1	2.1
1165	0.0	3.2U	2.8	1.4	1.2	0.7	1	0.15	NM	NM
1166	NA	NA	4.8	1.4	0.0	0.0	PP	PP	0.0	0.0
1167	0.0	6.2U	2.8	0.7	0.7	0.8	1	NM	NM	NM

Note: Negative shot number indicates the resulting data was not considered a "fair hit."

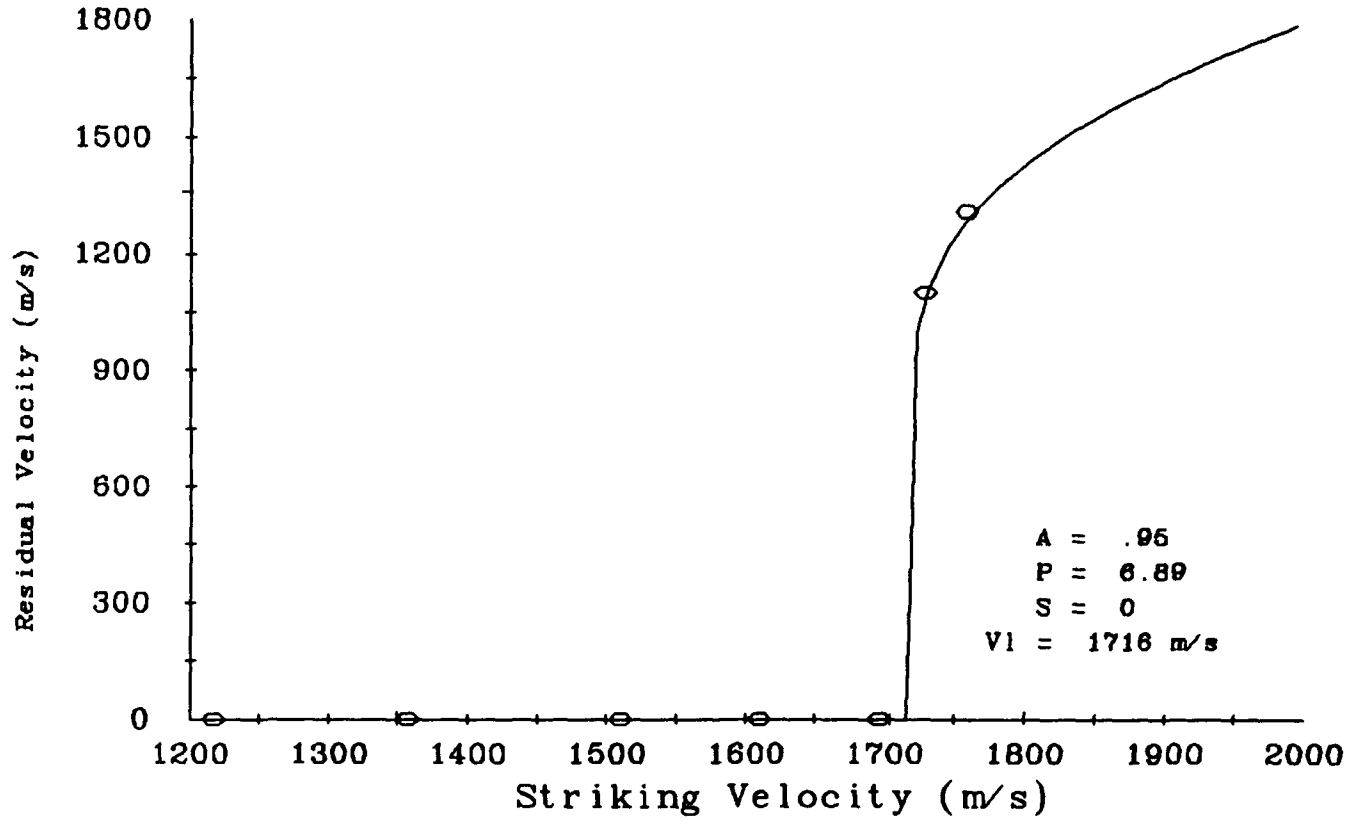

Figure B-3. V_s-V_r curve for the 0.60-cal. TBS against 31.75-mm RHA at 57° obliquity.

Table B-5. Individual Shot Data Tabulation for the 0.60-cal. TBS Against 12.7-mm RHA at 70.5° Obliquity

Series Fired 3 - 1992
Limit Velocity = 1,262, A = .99, P = 2.29, S = 255

Shot No.	α (°)	β (°)	γ (°)	V_s (m/s)	M_s (g)	η_R (°)	α_R (°)	V_r (m/s)	M_r (g)	Pen. (cm)
-1168	0.25U	0.50R	0.56	1,496	12.70	NA	NA	Lost	Lost	CP
1169	1.00U	0.25R	1.02	1,413	12.83	7.1U	NA	1,057 977	2.27	CP
1170	0.25U	0.50R	0.56	1,359	12.81	23.2U	NA	653	1.34	CP
1171	1.25U	0.25L	1.26	1,273	12.77	44.7U	NA	550 351	1.44 1.24	CP
1172	0.75D	0.50R	0.89	1,225	12.83	NA	NA	0	0.00	0.2
1173	0.25U	1.00R	1.02	1,246	12.83	NA	NA	0	0.00	0.4
1174	1.00D	0.25R	1.02	1,290	12.83	NA	NA	0	0.00	0.2
1175	0.0	0.25R	0.25	1,293	12.82	NA	NA	0	0.00	1.2

Note: Negative shot number indicates the resulting data was not considered a "fair hit."

Table B-5. Individual Shot Data Tabulation for the 0.60-cal. TBS Against 12.7-mm RHA at 70.5° Obliquity (continued)

Series Fired 3 - 1992
Limit Velocity = 1,262, A = .99, P = 2.29, S = 255

Shot No.	M.rec (g)	η_P (°)	V_{pl} (m/s)	M_{pl} (g)	M_{pr} (g)	L.p (cm)	W.p (cm)	Th. (cm)	EHL (cm)	EHW (cm)	Blg (cm)	Wt.L (g)
-1168	None BHN = 364	Lost	Lost	Lost	None	NM	NM	NM	2.7	1.1	0.0	105
1169	0.00 BHN = 364	NM	Lost	Lost	None	NM	NM	NM	2.7	1.1	NR	24
1170	0.00 BHN = 364	NM	Lost	Lost	None	NM	NM	NM	1.7	1.1	NR	17
1171	0.00 BHN = 364	89.6U	599	5.29	0.00	1.3	0.7	0.7	1.9	1.2	NR	6
1172	0.00 BHN = 364	NA	0	0.00	0.00	0.0	0.0	0.0	0.0	0.0	0.0	26
1173	0.00 BHN = 364	NA	0	0.00	0.00	0.0	0.0	0.0	0.0	0.0	0.1	11
1174	0.00 BHN = 0	NA	0	0.00	0.00	0.0	0.0	0.0	0.0	0.0	0.0	2
1175	0.00 BHN = 364	NA	0	0.00	0.00	0.0	0.0	0.0	0.0	0.0	0.3	20

Note: Negative shot number indicates the resulting data was not considered a "fair hit."

Table B-5. Individual Shot Data Tabulation for the 0.60-cal. TBS Against 12.7-mm RHA at 70.5° Obliquity (continued)

Series Fired 3 - 1992
Limit Velocity = 1,262, A = .99, P = 2.29, S = 255

Shot No.	Cone (°)	CoFS (°)	EntHL (cm)	EntW (cm)	CenL (cm)	CenW (cm)	No. Pcs.	M.R. Dia. (in)	BL (cm)	BW (cm)
-1168	Lost	Lost	4.0	1.3	1.2	0.7	Lost	Lost	0.0	0.0
1169	14.4	14.3U	3.7	0.8	0.9	0.7	0	0.00	NM	NM
1170	0.0	23.3U	4.3	0.7	0.9	0.7	0	0.00	NM	NM
1171	48.4	65.5U	2.8	0.7	1.0	0.6	3	0.00	NM	NM
1172	NA	NA	4.2	0.7	0.0	0.0	PP	PP	NM	NM
1173	NA	NA	4.6	1.1	3.8	0.0	PP	PP	0.1	0.1
1174	NA	NA	5.2	0.9	0.0	0.0	PP	PP	NM	NM

Note: Negative shot number indicates the resulting data was not considered a "fair hit."

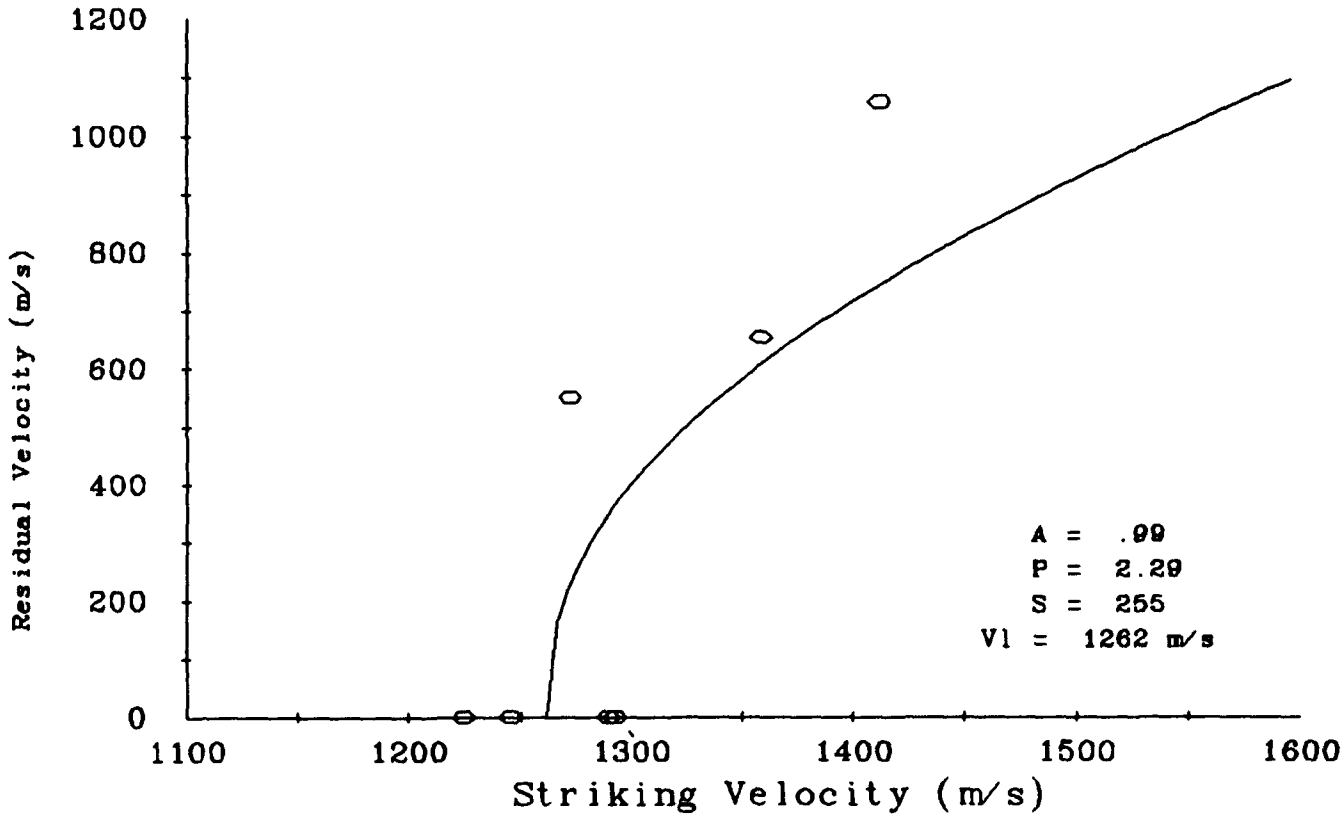

Figure B-4. V_s-V_r curve for the 0.60-cal. TBS against 12.7-mm RHA at 70.5° obliquity.

Table B-6. Individual Shot Data Tabulation for the 0.60-cal. TBS Against 19.05-mm HHA at 57° Obliquity

Series Fired 3 - 1992
Limit Velocity = 1,330, 2 Shot V_{50}

Shot No.	α (°)	β (°)	γ (°)	V_s (m/s)	M_s (g)	η_R (°)	α_R (°)	V_r (m/s)	M_r (g)	Pen. (cm)
1188	2.75D	0.75R	2.85	1,328	12.80	NA	NA	0	0.00	0.6
1189	0.50D	1.75L	1.82	1,416	12.92	74.2U	NA	0	0.00	CP
1190	2.25U	0.50R	2.30	1,373	12.82	39.2U	NA	567	1.03	CP
-1191	0.25D	1.25R	1.27	1,353	12.81	NA	NA	Lost	Lost	CP
-1192	0.25U	0.00	0.25	1,335	12.82	NA	NA	Lost	Lost	CP
-1193	Lost	Lost	Lost	Lost	12.83	NA	NA	Lost	Lost	CP
1194	0.50D	0.75L	0.90	1,333	12.81	19.6U	NA	414	NM	CP
1195	0.25U	0.00	0.25	1,330	12.83	38.2U	NA	428	7.50	CP

Note: Negative shot number indicates the resulting data was not considered a "fair hit."

Table B-6. Individual Shot Data Tabulation for the 0.60-cal. TBS Against 19.05-mm HHA at 57° Obliquity (continued)

Series Fired 3 - 1992
Limit Velocity = 1,330, 2 Shot V_{50}

Shot No.	M.rec (g)	η_P (°)	V_{pl} (m/s)	M_{pl} (g)	M_{pr} (g)	L.p (cm)	W.p (cm)	Th. (cm)	EHL (cm)	EHW (cm)	Blg (cm)	Wt.L (g)
1188	0.00 BHN = 512	NA	0	0.00	0.00	0.0	0.0	0.0	0.0	0.0	0.0	66
1189	0.00 BHN = 512	NM	264	6.58	0.00	1.1	1.0	0.8	1.3	1.2	NR	52
1190	None BHN = 512	78.1U	376	7.90	None	1.1	1.0	0.9	2.2	1.6	NR	21
-1191	None BHN = 512	70.7U	346 342	11.12	None	1.0	1.1	1.3	1.4	1.1	NR	34
-1192	None BHN = 512	61.5U	554 494	4.50	None	0.5	0.4	0.3	2.0	1.2	NR	5
-1193	0.00 BHN = 512	NM	413	9.09	0.00	1.3	1.2	0.8	2.0	1.1	0.0	22
1194	0.00 BHN = 512	19.9U	308	4.70	0.00	0.5	0.5	0.5	1.7	1.7	0.0	3
1195	0.00 BHN = 512	NM	424	4.50	0.00	1.1	0.8	0.7	2.0	1.3	0.0	24

Note: Negative shot number indicates the resulting data was not considered a "fair hit."

Table B-6. Individual Shot Data Tabulation for the 0.60-cal. TBS Against 19.05-mm HHA at 57° Obliquity (continued)

Series Fired 3 - 1992
Limit Velocity = 1,330, 2 Shot V_{50}

Shot No.	Cone (°)	CoFS (°)	EntHL (cm)	EntW (cm)	CenL (cm)	CenW (cm)	No. Pcs.	M.R. Dia. (in)	BL (cm)	BW (cm)
1188	NA	NA	3.9	1.3	NM	NM	0	PP	NM	NM
1189	2.4	73.0U	4.0	1.5	1.1	0.8	2	PP	NM	NM
1190	39.0	58.7U	3.4	1.4	0.8	0.8	2	NA	NM	NM
-1191	6.5	74.1U	3.5	1.4	1.0	0.8	2	NA	NM	NM
-1192	7.2	65.1U	3.1	1.3	1.1	0.7	2	NA	NM	NM
-1193	27.5	69.1U	3.2	1.4	1.0	0.8	2	PP	0.0	0.0
1194	5.8	22.3U	3.1	1.6	0.8	0.7	3	PP	0.0	0.0
1195	11.6	44.0U	3.1	1.4	0.9	0.8	2	PP	0.0	0.0

Note: Negative shot number indicates the resulting data was not considered a "fair hit."

Table B-7. Individual Shot Data Tabulation for the 0.60-cal. TBS Against 12.7-mm HHA at 70.5° Obliquity

Series Fired 3 - 1992
Limit Velocity = 1,431, A = .9, P = 2.99, S = 236

Shot No.	α (°)	β (°)	γ (°)	V_s (m/s)	M_s (g)	η_R (°)	α_R (°)	Vr (m/s)	Mr (g)	Pen. (cm)
1176	0.25D	0.50R	0.56	1,427	12.85	NA	NA	0	0.00	0.8
1177	0.00	0.00	0.00	1,433	12.71	41.6D	NA	728	2.41	CP
1178	0.25D	0.75R	0.79	1,431	12.68	NA	NA	0	0.00	0.3
1179	2.00U	1.00L	2.24	1,441	12.80	58.1U	NA	507	1.40	CP
1180	0.00	2.50L	2.50	1,438	12.76	NA	NA	0	0.00	NM
-1181	2.00D	0.75R	2.14	1,443	12.72	NA	NA	0	0.00	0.3
-1182	1.50D	1.00L	1.79	1,454	12.87	NA	NA	0	0.00	0.3
1183	2.00U	1.00R	2.24	1,483	12.83	48.7U	NA	594	7.90	CP
-1184	1.50D	0.50L	1.58	1,455	12.81	NA	NA	0	0.00	0.3
-1185	1.25D	2.25L	2.56	1,468	12.78	NA	NA	0	0.00	0.3
-1186	1.75D	1.25L	2.15	1,496	12.85	NA	NA	0	0.00	0.3
1187	2.25U	0.50R	2.29	1,512	12.80	26.8U	NA	792	1.25	CP

Note: Negative shot number indicates the resulting data was not considered a "fair hit."

Table B-7. Individual Shot Data Tabulation for the 0.60-cal. TBS Against 12.7-mm HHA at 70.5° Obliquity (continued)

Series Fired 3 - 1992
Limit Velocity = 1,431, A = .9, P = 2.99, S = 236

Shot No.	M.rec (g)	$\eta_{\neg}$ (°)	V_{pl} (m/s)	M_{pl} (g)	M_{pr} (g)	L.p (cm)	W.p (cm)	Th. (cm)	EHL (cm)	EHW (cm)	Blg (cm)	Wt.L (g)
1176	0.00 BHN = 512	NA	0	0.00	0.00	0.0	0.0	0.0	0.0	0.0	0.2	31
1177	0.00 BHN = 512	31.6D	808	3.18	0.00	1.1	1.0	0.4	2.3	1.5	NR	34
1178	0.00 BHN = 512	NA	0	0.00	0.00	0.0	0.0	0.0	0.0	0.0	0.0	4
1179	0.00 BHN = 512	44.0U	442	3.27	0.00	1.1	0.6	0.6	2.3	1.5	NR	10
1180	0.00 BHN = 512	NA	0	0.00	0.00	0.0	0.0	0.0	0.0	0.0	0.0	38
-1181	0.00 BHN = 512	NA	0	0.00	0.00	0.0	0.0	0.0	0.0	0.0	0.0	17
-1182	0.00 BHN = 512	NA	0	0.00	0.00	0.0	0.0	0.0	0.0	0.0	0.0	30
1183	0.00 BHN = 512	54.8U	490	4.36	0.00	1.8	1.3	0.2	3.0	1.6	NR	20
-1184	0.00 BHN = 512	NA	0	0.00	0.00	0.0	0.0	0.0	0.0	0.0	0.0	22
-1185	0.00 BHN = 512	NA	0	0.00	0.00	0.0	0.0	0.0	0.0	0.0	0.0	0
-1186	0.00 BHN = 512	NA	0	0.00	0.00	0.0	0.0	0.0	0.0	0.0	0.0	3
1187	0.00 BHN = 512	34.7U	799	3.95	0.00	0.8	0.8	0.9	3.4	1.8	NR	28

Note: Negative shot number indicates the resulting data was not considered a "fair hit."

Table B-7. Individual Shot Data Tabulation for the 0.60-cal. TBS Against 12.7-mm HHA at 70.5° Obliquity (continued)

Series Fired 3 - 1992
Limit Velocity = 1,431, A = .9, P = 2.99, S = 236

Shot No.	Cone (°)	CoFS (°)	EntHL (cm)	EntW (cm)	CenL (cm)	CenW (cm)	No. Pcs.	M.R. Dia. (in)	BL (cm)	BW (cm)
1176	NA	NA	5.2	1.3	NM	NM	PP	PP	2.6	1.0
1177	19.8	31.7D	4.2	1.9	1.0	0.8	3	NA	NM	NM
1178	NA	NA	3.6	1.0	NM	NM	PP	PP	0.0	0.0
1179	14.1	51.1U	4.8	1.0	1.5	0.7	1	NA	NM	NM
1180	NA	NA	4.1	1.2	NM	NM	PP	PP	0.0	0.0
-1181	NA	NA	4.0	0.9	NM	NM	PP	PP	0.0	0.0
-1182	NA	NA	4.5	1.0	NM	NM	PP	PP	0.0	0.0
1183	6.1	51.8U	5.1	1.5	2.0	0.7	2	NA	NM	NM
-1184	NA	NA	4.5	0.9	NM	NM	PP	PP	0.0	0.0
-1185	NA	NA	3.5	3.5	NM	NM	PP	PP	0.0	0.0
-1186	NA	NA	4.3	1.0	NM	NM	PP	PP	0.0	0.0
1187	7.8	30.8U	5.0	1.5	1.7	0.9	1	0.00	NM	NM

Note: Negative shot number indicates the resulting data was not considered a "fair hit."

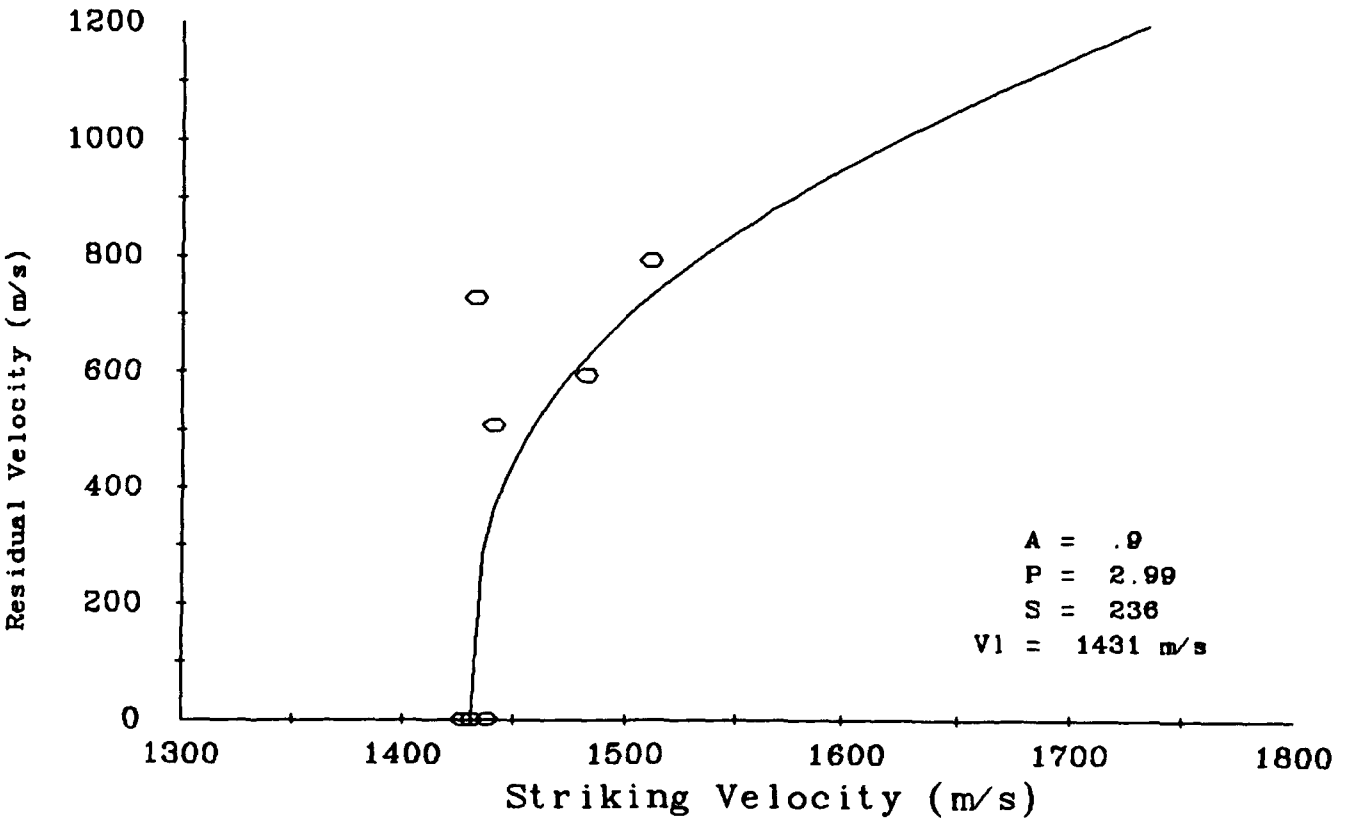

Figure B-5. V_s-V_r curve for the 0.60-cal. TBS against 12.7-mm HHA at 70.5° obliquity.

INTENTIONALLY LEFT BLANK.

No. of Copies	Organization
2	Administrator Defense Technical Info Center ATTN: DTIC-DDA Cameron Station Alexandria, VA 22304-6145
1	Commander U.S. Army Materiel Command ATTN: AMCAM 5001 Eisenhower Ave. Alexandria, VA 22333-0001
1	Director U.S. Army Research Laboratory ATTN: AMSRL-OP-CI-AD, Tech Publishing 2800 Powder Mill Rd. Adelphi, MD 20783-1145
1	Director U.S. Army Research Laboratory ATTN: AMSRL-OP-CI-AD, Records Management 2800 Powder Mill Rd. Adelphi, MD 20783-1145
2	Commander U.S. Army Armament Research, Development, and Engineering Center ATTN: SMCAR-IMI-I Picatinny Arsenal, NJ 07806-5000
2	Commander U.S. Army Armament Research, Development, and Engineering Center ATTN: SMCAR-TDC Picatinny Arsenal, NJ 07806-5000
1	Director Benet Weapons Laboratory U.S. Army Armament Research, Development, and Engineering Center ATTN: SMCAR-CCB-TL Watervliet, NY 12189-4050
1	Director U.S. Army Advanced Systems Research and Analysis Office (ATCOM) ATTN: AMSAT-R-NR, M/S 219-1 Ames Research Center Moffett Field, CA 94035-1000

No. of Copies	Organization
1	Commander U.S. Army Missile Command ATTN: AMSMI-RD-CS-R (DOC) Redstone Arsenal, AL 35898-5010
1	Commander U.S. Army Tank-Automotive Command ATTN: AMSTA-JSK (Armor Eng. Br.) Warren, MI 48397-5000
1	Director U.S. Army TRADOC Analysis Command ATTN: ATRC-WSR White Sands Missile Range, NM 88002-5502
(Class. only) 1	Commandant U.S. Army Infantry School ATTN: ATSH-CD (Security Mgr.) Fort Benning, GA 31905-5660
(Unclass. only) 1	Commandant U.S. Army Infantry School ATTN: ATSH-WCB-O Fort Benning, GA 31905-5000
1	WL/MNOI Eglin AFB, FL 32542-5000
	Aberdeen Proving Ground
2	Dir, USAMSAA ATTN: AMXSY-D AMXSY-MP, H. Cohen
1	Cdr, USATECOM ATTN: AMSTE-TC
1	Dir, ERDEC ATTN: SCBRD-RT
1	Cdr, CBDA ATTN: AMSCB-CII
1	Dir, USARL ATTN: AMSRL-SL-I
10	Dir, USARL ATTN: AMSRL-OP-CI-B (Tech Lib)

No. of Copies	Organization
2	Commander U.S. Army Armament Research, Development, and Engineering Center ATTN: SMCAR-FSE, Riccardo Brognara Mr. William H. Davis Bldg. 329 Picatinny Arsenal, NJ 07806-5000
5	Commander U.S. Army Armament Research, Development, and Engineering Center ATTN: SMCAR-CCL-FA, H. Moore H. Kahn W. Williams B. Schlenner MAJ Gus Gerasimas Bldg. 65N Picatinny Arsenal, NJ 07806-5000
1	Director Benet Laboratories ATTN: SMCAR-CCB-RT, Peter D. Aalto SMCAR-CCB-RM, Dr. Pat Votis Watervliet, NY 12189
3	CG, MCRDAC Code AWT ATTN: Dr. C. Vaughn Mr. G. Solhand MAJ F. Wysocki Quantico, VA 22134-5080
2	IAP Research, Inc. ATTN: Dr. John P. Barber Mr. David P. Bauer 2763 Culver Ave. Dayton, OH 45429-3723
2	LTV Aerospace and Defense Company ATTN: MS TH-83, Dr. Michael M. Tower Dr. G. Jackson P.O. Box 650003 Dallas, TX 75265-0003

No. of Copies	Organization
1	Science Applications International Corporation ATTN: Dr. K. A. Jamison 1247-B North Eglin Parkway Shalimar, FL 32579
1	FMC Corporation Mailstop M170 ATTN: Brad Goodell 4800 East River Rd. Minneapolis, MN 55421-1498
2	Institute for Advanced Technology The University of Texas at Austin ATTN: Dr. Harry Fair Dr. Tom Kiehne 4030-2 W. Braker Ln. Austin, TX 78759-5329
1	Center for Electromechanics University of Texas at Austin ATTN: Mr. John H. Price 10100 Burnet Rd., Bldg. 133 Austin, TX 78748
2	Kaman Sciences Corporation ATTN: Mr. Doug Elder Mr. Tim Hayden 1500 Garden of the Gods Road P.O. Box 7463 Colorado Springs, CO 80933
18	Aberdeen Proving Ground Dir, USARL ATTN: AMSRL-WT-TD, Tim Farrand (5 cps) Konrad Frank AMSRL-WT-TC, Lee Magness Wendy Leonard Randolph Coates Bill de Rossett Todd Bjerke Eleanor Deal Graham Silsby AMSRL-WT-TA, Matt Burkins Bill Gooch AMSRL-WT-WD, Alex Zielinski (3 cps) AMSRL-WT-PB, James Garner

USER EVALUATION SHEET/CHANGE OF ADDRESS

This Laboratory undertakes a continuing effort to improve the quality of the reports it publishes. Your comments/answers to the items/questions below will aid us in our efforts.

1. ARL Report Number ARL-MR-104 Date of Report September 1993

2. Date Report Received _____

3. Does this report satisfy a need? (Comment on purpose, related project, or other area of interest for which the report will be used.) _____

4. Specifically, how is the report being used? (Information source, design data, procedure, source of ideas, etc.) _____

5. Has the information in this report led to any quantitative savings as far as man-hours or dollars saved, operating costs avoided, or efficiencies achieved, etc? If so, please elaborate. _____

6. General Comments. What do you think should be changed to improve future reports? (Indicate changes to organization, technical content, format, etc.) _____

CURRENT ADDRESS

_____
Organization

_____
Name

_____
Street or P.O. Box No.

_____
City, State, Zip Code

7. If indicating a Change of Address or Address Correction, please provide the Current or Correct address above and the Old or Incorrect address below.

OLD ADDRESS

_____
Organization

_____
Name

_____
Street or P.O. Box No.

_____
City, State, Zip Code

(Remove this sheet, fold as indicated, tape closed, and mail.)
(DO NOT STAPLE)

DEPARTMENT OF THE ARMY

OFFICIAL BUSINESS

BUSINESS REPLY MAIL
FIRST CLASS PERMIT No 0001, APG, MD

Postage will be paid by addressee

NO POSTAGE
NECESSARY
IF MAILED
IN THE
UNITED STATES

Director
U.S. Army Research Laboratory
ATTN: AMSRL-OP-CI-B (Tech Lib)
Aberdeen Proving Ground, MD 21005-5066